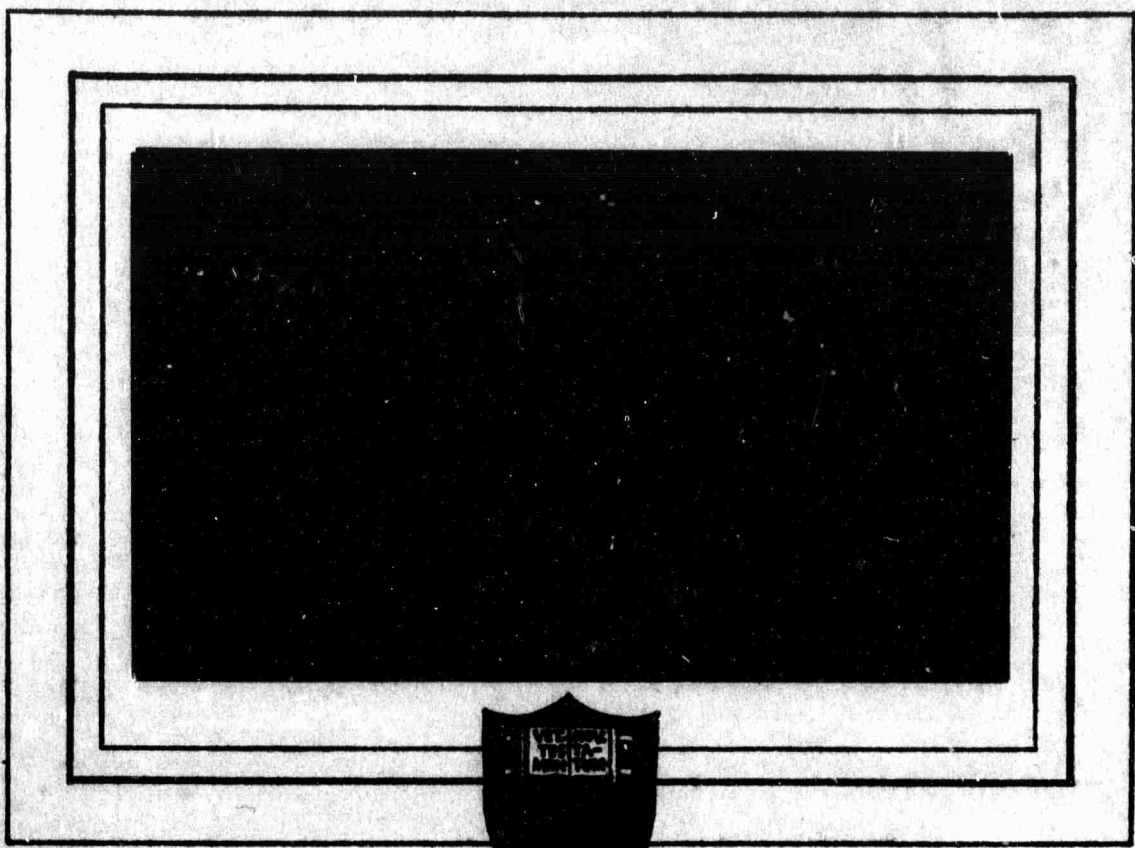


AD 674606



This document has been approved for public release and sale; its distribution is unlimited

# PRINCETON UNIVERSITY

Reproduced by the  
CLEARINGHOUSE  
for Federal Scientific & Technical  
Information Springfield Va. 22151

DDC  
RECORDS  
SEP 18 1968  
ALBANY

DIFFRACTION OF P BY THE CORE:  
A STUDY OF LONG-PERIOD AMPLITUDES  
NEAR THE EDGE OF THE SHADOW

Robert A. Phinney  
Lawrence M. Cathles

Dept. of Geological and Geophysical Sciences

Semi-annual technical summary  
Contract AF 49 (638) - 1243

Advanced Research Projects Agency  
ARPA Order No. 292

30 June 1968

**BLANK PAGE**

**DIFFRACTION OF P BY THE CORE: A STUDY OF LONG-PERIOD  
AMPLITUDES NEAR THE EDGE OF THE SHADOW.**

**Robert A. Phinney**

**Lawrence M. Cathles**

### Abstract

Theoretical expressions for the amplitude of P-waves in the neighborhood of the core shadow boundary have been formulated and evaluated by computer. Comparison with 2.5 second data of Sacks confirms his determination of the shadow position at  $96.5^\circ$ . A square root frequency scaling law is found for the high frequency diffraction pattern, and permits use of the Fresnel integral function at short periods. Long-period amplitude data for three paths have been spectrum analyzed and compared against the theoretical amplitude dropoff going into the shadow. The agreement is about as good as the data will permit, and no indication is found at these periods of a low-amplitude defocused region at  $90^\circ$  to  $96^\circ$ , after diffraction has been accounted for.

### Introduction

The penetration of long-period P waves deep into the optical shadow of the core by diffraction is a familiar demonstration that the amplitudes predicted by geometrical optics do not apply for a wide range of periods. The work reported here is part of a larger study aimed at developing useful wave-theoretical models of body wave amplitudes near singularities of the travel time curves. The specific problem of the core shadow is recognizably analogous to familiar problems of mathematical physics, namely the shadowing of light by an opaque screen and the diffraction of waves around a sphere.

Mathematical techniques appropriate to the problem of diffraction by a sphere were developed by Watson (1918) and by Van der Pol and Bremmer in a series of papers (Bremmer, 1949). Scholte (1956) and Duwalo and Jacobs (1956) first applied these ideas to the elastic wave problem, and Nussenzweig (1965) treated the basic acoustic diffraction problem with great thoroughness, giving asymptotic solutions for all the relevant receiver positions. Teng and Wu (1968) have worked with a two-dimensional ultrasonic model, providing analog solutions which agree with results given in this paper.

The simplest kinematical property of the core diffraction is the spatial decay constant of the wave which illuminates the deep shadow by propagation along the core-mantle interface. Phinney and Alexander (1966) obtained theoretical curves for this parameter

for various models of the core-mantle boundary. Alexander and Phinney (1966) investigated the frequency dependence of the decay constant for long-period data from a selection of earthquakes.

The principal results of these two papers were:

a) The determination that rigidity in the core has no significant effect on the decay constant, for the low rigidities known to be present.

b) The presence of apparent resonance maxima in the decay constant as a function of frequency for a group of paths over the Pacific, and the absence of this effect for a path from South America to Europe. Interpretation in terms of a transitional region at the core-mantle interface suggested a reduced shear velocity and increased density with respect to the mantle.

Serious questions still exist regarding this interpretation, connected with the repeatability of the results and the sensitivity of the results to stations with inadequately calibrated response (including a local geological correction). While two more profiles will be discussed in this paper, a more comprehensive study will be presented in a separate paper (Alexander and Phinney, in preparation).

In this paper we discuss the behavior of the P-wave amplitude at distances which span the optical shadow position. We present calculations of the theoretical amplitude decay in this region and discuss the amplitude and phase velocity effects which arise from the diffraction. Some estimate can be made of the frequency

and distance ranges for which ordinary ray theory and conventional time-domain amplitude analysis are valid. The distance of the optical shadow is estimated from published short-period data, and confirms Sack's (1966) determination of about  $96.5^\circ$ . A comparison of the theoretical amplitudes with an approximation based on diffraction by an opaque screen provides a usable amplitude function for high frequencies ( $f > .12$  hz).

For comparison, long period data from two earthquakes, spanning three paths, have been frequency analyzed and plotted as residuals against the theoretical amplitudes. The agreement is found to be quite good, although small effects are found which may be connected with departures from a simple model of the interface. Further study of these effects will require far better inter-station calibration (including a crustal correction) and simultaneous determination of a source mechanism model. Since no provision is made in this paper for velocity variation in the mantle, we have not modeled beyond the reversal in velocity gradient at the base of the mantle. This reversal is indicated by the observed amplitude drop beyond  $85^\circ$  assuming a geometrical optical mechanism. The lack of an amplitude residual in this range for long periods suggests that diffraction accounts fully for the long period amplitude drop. Our results, therefore, do not seem to require any basal mantle structure to provide additional defocusing. The low resolution provided by the long periods does not make this an especially strong result, however.

### Theory

Assume an earth consisting of a homogeneous elastic mantle and a homogeneous liquid core. With the origin of spherical coordinates at the center of the earth, the representation of a compressional point source at the surface is (Phinney and Alexander, 1966):

$$\Phi_0 = \frac{e^{ikR}}{ikR} = \sum_{n=0}^{\infty} (2n+1) P_n(\cos\theta) h_n^{(1)}(k_0 b) \hat{j}_n(k_0 r) \quad (1)$$

In discussing diffraction by the core, the outer boundary of the earth may be ignored, provided the frequency is high enough for rays to be separated in the time domain. The diffracted signal, which includes both the incident wave and the generalized reflection from the core is then:

$$\Phi = \frac{1}{2} \sum_{n=0}^{\infty} (2n+1) P_n(\cos\theta) h_n^{(1)}(k_0 b) \left[ h_n^{(2)}(k_0 r) + C_0' h_n^{(1)}(k_0 r) \right] \quad (2)$$

By applying a modification of the transformation of Watson<sup>4</sup>, we may write the diffraction as a sum of forward and backward-traveling waves which have made  $\underline{m}$  circuits of the origin. For the forward-traveling wave with  $m = 0$ , we have:

$$\Phi = \int_{-\infty}^{\infty} Q_{\nu-\gamma_2}^{(2)}(\cos\theta) \frac{N(\nu)}{D(\nu)} \nu d\nu \quad (3)$$

By taking the asymptotic forms of the various expressions in the integrand for large  $\nu$  and fixed  $ka$ , we find that all the terms except  $m = 0$  can be evaluated by moving the contour into the upper half plane and writing the integral as a sum of residues. The residue sum associated with the  $m$ th term is a "creeping wave" which has made  $m$  transits of the origin, along the core-mantle boundary at the mantle P-velocity. The  $m=0$  term can be written as a convergent residue sum only if the receiver is in the geometrical shadow of the core, in which case, the term represents the principal diffracted P wave in the shadow, having made less than one complete trip around the origin. If the receiver is in the illuminated zone, examination of the asymptotic form of (3) reveals two saddle points on the real  $\nu$ -axis, which correspond to the reflected and direct waves. When the receiver is very close to the shadow boundary, these saddle points approach each other. Formal discussion of this signal is possible only for frequencies high enough that the asymptotic expansions can be relied upon.

Because of our desire to have reliable numerical results, and to generalize them to a core-mantle boundary having layers or other radial structure, we have programmed (3) directly on the IBM 7094 and evaluated it by line integration along an optimum path. The path is generally arranged to be a steepest descent path at its extrema and to connect the two saddle points along the real axis.

Since line integration is suitable for (3) even if the receiver is in the shadow, we routinely continue the evaluation into the shadow zone, where we can compare the result with the residue theory for the first pole. Typical maps of the complex plane are shown in Figure 1. The saddle points and steepest descent contours are indicated, and the function contoured is the  $\text{Re}[\ln(\text{integrand})]$ , which is just the function whose steepest descent is of interest.

Because of the constant phase along the steepest descent paths, a Simpson or other low order integration method is adequate. The variable phase between the two saddle points is not a severe limitation, provided the two points are not too separated. When they are separated, the signals P and PcP are sufficiently distinct in time that this combined approach is unnecessary. For example, at a fixed distance from the shadow, the frequency can be made high enough that the two saddle points are distinct, which corresponds to the fact that the small time separation can be seen at such high frequencies. Numerical checking of the program included runs using different contours, runs around the poles, runs around closed loops, etc. The fractional error appears to be around 0.1% of the amplitude computed.

#### Numerical results:

In all cases, the following parameters were used

source and receiver radius:  $6350 \text{ km} = r$

core radius:  $3480 \text{ km} = a$

mantle: P-velocity 13.6 km/sec  
 S-velocity 7.5 km/sec  
 density 5.5

for "model 1" the core properties are

P-velocity 8.3 km/sec  
 S-velocity .001 km/sec  
 density 9.5

for "mixed boundary condition" (M),  $u_r$  and  $\tau_{r\theta}$  vanish at  $r=a$ .

for "hollow boundary condition" (H),  $\tau_{rr}$  and  $\tau_{r\theta}$  vanish at  $r=a$ .

The shadow position for this model is at  $113.54^\circ$ . A normalized frequency of  $ka=100$  corresponds to a true frequency of .0622 and a true period of 16.1 sec.

At distances beyond the shadow boundary the first pole was located and the residue evaluated at the pole as a check on the numerical integration. As expected, the two results converge as the receiver moves to larger distances.

In Figure 2 we have plotted the diffraction amplitude (as  $\log_e$ ) against epicentral distance for "model 1", our reference earth model. For comparison the amplitude of the direct wave ( $1/kR$ ) is shown. In the illuminated zone away from the shadow, the diffraction pattern appears as the incident wave amplitude with a superposed ripple due to the addition of the PcP signal. The ripple is small enough that only a very well-calibrated array could detect it; this being due to the fact that the P-P reflection coefficient is not great. At a certain critical distance from the

shadow, the screening effect of the core comes into play, and the amplitude begins to drop rapidly. The rate of falloff with distance in the transition zone near the shadow is greater than the normal deep-shadow decay given by the lines for the residue solution. This suggests that experimental determination of the deep-shadow decay may be biased by using stations too close to the shadow. The author is not unmindful that the earlier work with Alexander is subject to this effect, which was allowed for at the time, but was not known numerically.

If the ripple is ignored, these curves resemble the data obtained by Sacks (1966), in having a monotonic  $1/R$  decrease in the illuminated zone, followed by a sharper monotonic decrease into the shadow. Sacks suggested that the shadow position could be located by identifying the break point at shorter periods, where diffraction effects should be unimportant. We now have a basis for identifying the shadow position at any period by applying a correction to the location of the break point.

Simple physical arguments are available to demonstrate that this break in slope should occur in the illuminated zone, and to provide a scaling law, valid for "high frequencies". Consider (Figure 3) a model in which the core is replaced by an opaque screen, and assume that the Kirchhoff integration method is adequate to provide the total field at the receiver. It is then appropriate to set up Fresnel zones in the plane of the screen

and to inquire at what distance the receiver must lie from the shadow boundary for the first zone to lie off the screen. If we assume that  $\phi$  is small, then the path length difference  $BA - BA'R$  which defines the edge of the first zone is given by

$$\phi \approx \left( \frac{1}{2} \frac{\lambda}{BAR_s} \right)^{1/2}$$

This gives a square root scaling law for features in the diffraction pattern near the shadow boundary. Expressed as a discrepancy in the epicentral distance, we have

$$\Delta\theta \cong 2\phi = \left( \frac{2\pi}{ka} \frac{a}{r \sin \frac{1}{2}\theta_s} \right)^{1/2} \approx 2.0 (ka)^{-1/2} = 114.2^\circ (ka)^{-1/2} \quad (4)$$

In Figure 4, this relationship is plotted along with plots of two of the characteristic features of the diffraction pattern: the distance from breakpoint to shadow and the distance from first peak to shadow. The validity of the square root law at higher frequencies is verified, although the simplifications in the Fresnel zone model give a modest difference in the actual shift. The square root scaling law enables a projection to shorter periods, and an estimate to be made of the distance between

shadow boundary and breakpoint. Extrapolations to periods of 1.6, 1.0 and 0.5 sec. give values for the shift of  $3.1^\circ$ ,  $2.4^\circ$ , and  $1.7^\circ$ , respectively.

Figures 6 and 7 give the theoretical diffraction amplitude for a "mixed" and a "hollow" core, respectively. A comparison of various models is afforded in Figure 8. As mentioned previously (Phinney and Alexander, 1966), the "mixed" boundary condition is the simple model which best approximates the actual situation. Neither looks much like the result for a rigid or hollow core. The close resemblance between the latter two is in agreement with Knopoff and Gilbert (1961), who found the rigid and hollow cores indistinguishable from the view of geometrical diffraction theory.

From these results it is possible to infer changes in the shape of the spectrum of a pulse as it transits the shadow edge. At points a few degrees inside the illuminated zone frequencies lower than a certain value are attenuated with respect to the higher frequencies; this is due to the screening of the low frequencies for which the receiver is in the first Fresnel zone. The spectrum is thus relatively enriched in the high frequencies at such points. At the shadow edge, all frequencies are down by about the same amount, thus restoring the original pulse spectrum, and in the nonilluminated region the high frequencies are more rapidly attenuated, giving a spectrum relatively richer at low

frequencies. The magnitude of this effect in the illuminated zone is at best about 20%, however.

Comparison with asymptotic theory: By taking the frequency sufficiently high, one may form asymptotic expressions for the wave amplitude in various regions. Nussenzweig's (1965) treatment of the acoustic problem may serve as a model for this analysis in the elastic wave problems of interest. A complete treatment has been performed, but is beyond the scope of this paper; we report only the main results. Three regions may be distinguished:

a) Illuminated zone:

$$(\theta_s - \theta) \gg (ka)^{1/3}$$

The signal at the receiver is composed of the sum of direct P and reflected PcP, with phases, amplitudes, and reflection coefficients determined by ray theory.

b) Transition zone:

$$(\theta - \theta_s) \ll (ka)^{1/3}$$

The signal may be described by the Fresnel integral, which gives the classical diffraction pattern of a straight edge, plus a small correction term. Teng and Richards (1968) have investigated this theory and expressed their results in terms of an effective shift of the shadow position. These authors have compared their results with the calculations here reported and we will not duplicate this discussion.

c) Shadow zone:

$$(\theta - \theta_s) \gg (ka)^{1/3}$$

The signal is composed principally of a pole contribution, corresponding to a pulse diffracted along the core-mantle boundary with a given decay constant. The properties of this signal have already been discussed (Phinney and Alexander, 1966).

What is of interest in this paper is the determination of a useful form for the amplitude at high frequencies, which gives the transition to shadow. Unfortunately, the above cited theory, while valid separately in three regions, is deficient in the gaps between these regions.

What we will show here is that, despite the theoretical existence of a shadow shift and the theoretical deficiency in patching the regions together, the Fresnel integral so dominates the behavior of the amplitude that it gives a perfectly good representation of our higher frequency results by itself. This term, as it appears in this problem, has the form:

$$\phi = \frac{e^{-ikR}}{ikR} D(\Theta) \quad (5)$$

where:

$$D(\Theta) = 1 - e^{-i\pi/4} \sqrt{2} \int_0^{\Theta} \exp\left[\frac{i\pi\tau^2}{2}\right] d\tau \quad (6)$$

$$\Theta = \sqrt{\frac{kR}{4T}} (\theta - \theta_s)$$

is the Fresnel integral (Abramowitz and Stegun, 1965) which, by itself, gives the amplitude in the neighborhood of an opaque screen. It is seen that (5) provides the square root scaling inferred on physical grounds in a previous paragraph. In Figure 9 we show the Model 1 theoretical curves for  $ka=200$  and  $600$ , and compare them with (6). The amplitudes are arbitrarily taken equal at the shadow position; if they were matched by the ray-theoretical values at the shadow, a slight shift of the patterns would be seen. In any case, we find that the Fresnel integral can be used as a short period representation, for periods less than about 8 seconds, with errors that lie in the noise of existing data networks.

Insert Table 1 here

The other models of the core-mantle boundary do not show as good an agreement (compare Figures 8 and 9). The elastic parameters of the real earth seem fortuitously to give the ideal behavior of an opaque screen. This may be understood by noting that the acoustic impedances  $\rho c$  of core and mantle are quite well matched, resulting in relatively little reflection by the boundary. If this reflection is ignored, the field at a receiver may be expressed as a Fresnel-Huygens integral over the portion of the wavefront not screened by the core, leading directly to (5). (Born and Wolf, 1965).

The shadow position: It is clear that shorter periods must be used to make any kind of precise determination of the shadow position. The data discussed later in this paper are all long period, so we will rediscuss the results reported by Sacks (1966). He measured amplitudes in the time domain, taking signals which were band-limited by the seismometer. To the extent that the amplitudes of these wave packets are good estimates of Fourier amplitudes, his plot of amplitude decay at three periods is a proper one. The frequency dependent resonances due to structure found by Alexander and Phinney (1966) are certainly minor, and offer some reason to believe that Sacks' results are a good representation. Other difficulties with this time domain frequency analysis may arise in the illuminated zone, due to the lagged superposition of P and PcP, but here the small PcP reflection coefficient minimizes the problem.

In Figure 5, Sacks' results are plotted for comparison with our computed diffraction patterns. Two degrees of freedom are available...the amplitude and the angle scale. Since we have made no independent determination of the frequency content of the signal, the scale factor for each frequency is arbitrary, and may be chosen to get a good fit. The two angle scales are not the same, since the theoretical model does not take account of the variable velocity in the mantle and has a different

position for the shadow. Knowing that the distortion of wave fronts by the velocity distribution in the lower mantle is not "too severe", we find that the error involved in simply translating the theoretical curve a few degrees to match the position of the shadow with that of the real earth is acceptably small. [Future data analyses may require that the mantle structure be included in the theory in a reasonable way]. A full discussion of this point may be based on a WKBJ treatment of the wave function in the mantle.

The placement of the theoretical curves on Figure 5 is done in the following way:

a) The amplitude of the theoretical curve for 2.6 seconds is scaled to agree with the data at  $80^\circ$ , which is in the illuminated zone. The ripple being small, the theoretical curve here is just  $1/kR$ , which fortuitously decays in about the same way as real ray amplitudes in this region. The abscissa is now shifted to afford the best agreement with the data in the shadow. The fit in shape is good as the data scatter will permit. The abscissa shift brings the shadow position to  $96.5^\circ$ .

b) The theoretical curve for 25 seconds is directly plotted, using the scale adjustments determined for the 2.5 second data. Beyond  $86^\circ$  the fit is quite good. Since an independent amplitude adjustment was not necessary, we have coincidentally found that the spectrum of the earthquake had the  $1/k$  (step) behavior assumed in the theoretical model, with respect to these two periods.

c) Using the Fresnel integral we can construct a theoretical pattern for 0.7 seconds. If plotted using the scale adjustments of the 2.5 second data, the amplitude would be too large by a factor of 12. Making an independent amplitude shift, then, we plot the theoretical 0.7 curve to match the data in the illuminated zone. The dropoff of amplitude into the shadow is seen to take place at the right distance.

While the 25 second and 0.7 second results are interesting, the 2.5 second result is more constrained, due to the availability of data on both sides of the break in slope and to the sharpness of the break. To the extent that a single interface is a good model of the core-mantle boundary, we find a shadow position of  $96.5^\circ$ , essentially in agreement with Sacks.

It is worth noting that precise knowledge of the shadow position is not equivalent to a better determination of core radius. Either the velocity profile at the base of the mantle or the radius of the core may be independently adjusted to bring about a desired shadow position. The very different effect of the velocity profile on near-vertical PcP and on near-grazing P indicates the desirability of a study which jointly rationalizes both types of data. A number of authors have contributed to this problem in the past few years. In this paper no position is taken regarding the core radius.

Analysis of data: To provide some notion of the behavior of real amplitudes for comparison with the theory, data from two earthquakes, involving three different paths, have been analyzed to determine the behavior of their Fourier components near the shadow boundary. Tables 3 and 4 and Figures 10, 14, and 18 characterize the sources and array characteristics. As far as permitted by the distribution of stations, each analysis was chosen to involve a restricted range of azimuths, and thus to eliminate effects of the radiation pattern.

Preliminary processing involved digitizing (about 1/sec), and removal of trend for a time window somewhat in excess of the pulse length. For these two events the reverberation following the pulse is low enough that selection of a cutoff offers no problems, and the spectrum can be regarded as a Fourier integral spectrum, defined for continuous frequency, but smooth according to the pulse length. The presentation of the results for frequencies of .02, .03....., .07 reflects the band containing significant energy and the limited number of independent spectral values possible for the time window used. Amplitude calibration was employed for the LRSM data, using information supplied with the data. USCGS World-Wide Network data was taken from 15x reproductions of the 70 mm film chips; the nominal magnification was used for calibration unless the calibration pulse fell outside 10% limits. Stations with anomalous calibration time con-

stants were not used. This approach follows our observation that most of the scatter in the final results was not attributable to instrument calibration (or radiation pattern, for that matter). Other stations were deleted due to high noise levels, unstable base lines, or grossly unexplainable discrepancies.

The data were then Fourier transformed. Figures 11, 15, and 19 show representative time signals and their amplitude spectra. It is then appropriate to form a plot of amplitude for each frequency as a function of distance. Diffraction amplitudes must look very much like those shown in Figure 2, with possible perturbations superposed, due to departures from the Model 1 earth. Consequently, they are plotted as residuals against the nominal Model 1 diffraction amplitudes. This processing requires:

- a) The theoretical amplitudes are transformed to natural logarithms, and  $\frac{1}{2}\ln(\sin \Theta)$  subtracted, to eliminate focusing due to the spherical geometry. This scale is taken so that the ray-theoretical amplitude  $1/kR$  is at zero for  $\Theta = 90^\circ$  (model 1 earth). These functions, tabulated in Table 2, may be used as a standard for comparison of data.
- b) The experimental amplitudes are transformed to natural logarithms, and similarly corrected for focusing. The

scale is set to zero at a selected station in the illuminated zone.

c) The residual, experimental - theoretical, is formed, and plotted, in Figures 12, 16, and 20. For this purpose, the theoretical pattern is shifted to give a shadow position of  $96.5^\circ$ , in agreement with our discussion of the 2.5 second results.

A special problem exists in plotting the results from two networks together, due to the differing instrument responses. In this case, for Taiwan to North America, Figure 16, one assumes that the signal is identical at two proximate stations from the two networks, and corrects all LRSM spectral amplitudes to the USCGS response on the basis of the observed spectra at the two stations. GOL and DRCO were used for this adjustment; other proximate station pairs, such as LUB - HBOK and BLA-BLWV then plot with good agreement, providing some validation to the procedure.

Discussion: These results are plotted in a way which permits small effects in the ordinates, including scatter, to be amplified. The main effect is agreement with the theoretical diffraction, manifest as points lying on a horizontal. Further systematic effects, due to structure of some sort in the core-mantle region, should be apparent, if present and if proper allowance could be made for the crust-upper mantle correction at each station.

As mentioned, we find that refined calibration does not reduce the scatter, which amounts to .2 - .4, or about 3 db. The present advisability of a correction for crustal response (Haskel, 1962), may be questioned. It may be shown (Alexander and Phinney, 1966) that to first order all stations have the same crustal correction to 10%, in this long-period band, due to their situation on crust of approximately the same thickness. While admittedly unsatisfactory, we find this preferable to applying P-wave spectral corrections which are based on an extremely heterogeneous body of information about crustal structure. The only consistent way to make this correction is to use the P-waves themselves as calibrators, using a variety of earthquakes, and studying ratios between station pairs and between individual components. It is quite likely that a major cause of amplitude variation is scintillation caused by velocity heterogeneity in the upper mantle. Short period amplitude and travel time calibration of the LASA array in Montana (Broome, 1967) encourages this view, and demonstrates the strong dependence of the corrections on azimuth and angle of incidence.

Certain anomalies in the amplitude residuals might be discerned, although we do not insist too strenuously on their reality. The best of these is a pronounced increase in the decay rate in the shadow, seen at .06 hz in the Brazil - Europe analysis

(Figure 12). Figures 13 and 17 show an analysis of this decay for the two regions having suitably located stations. Aside from the .06 point, which appears real, and which might be explained with the requisite ingenuity, the remainder of the Brazil decay spectrum is quite nominal, a confirmation of the result for this path obtained by Alexander and Phinney (1966). The Taiwan - North America decay spectrum (Figure 17) is anomalously high, again in agreement with the earlier results from the North Pacific, although the reader can judge the degree to which this result is dependent on the choice of stations for analysis. In either case, one may discern a drop of .3 - .5 in the residual around  $105^\circ$ . Such an effect, if real, cannot be due to perturbations in the shadow position produced by variations in lower mantle structure; that is ruled out by the drop being sharp at these long periods. One can postulate a lateral reflector scatterer at the base of the mantle or a major region of defocusing due to shallower mantle inhomogeneity.

Teng (1968) studied the Q structure of the lower mantle by comparing spectra within a group of stations. The question of whether his data requires a low-Q zone at the base of the mantle hinges on the extent to which diffraction effects were fully accounted for. Data scatter is a problem here, too. A full correction would require taking residuals with respect to our nominal diffraction amplitudes before computing the  $Q$ -related effects.

We have shown that diffraction effects penetrate several degrees (depending on frequency) into the illuminated zone, giving an amplitude drop of a factor of 2 in this region. Amplitude decrease beyond about  $85^\circ$  has long been noticed in conventional P-wave amplitude studies which use time domain measurements and ray theory interpretations. It is not possible to convert such published amplitudes into a form comparable with the frequency-dependent theory. Some discussion is still possible. We note that the square root scaling of the diffraction pattern at intermediate and high frequencies implies relatively little shift in the pattern the higher the frequency. Even at 1 hz, normally used in amplitude studies, the amplitude is expected to begin dropping  $2.5^\circ$  short of the shadow position. Figure 21 compares a recent amplitude curve by Cleary (1967) with diffraction theory for .03 and .25 hz. If the signals used were in this frequency range, then diffraction may fully account for the observations. Cleary also found essential agreement between their observed travel times  $\left(\frac{d^2T}{d\theta^2}\right)$  on a ray theoretical interpretation.

Since amplitude distortion implies phase distortion in a linear realizable system, we may determine the departures of the P-wave phase velocity from ray theory, directly from the originally computed phase spectrum. Figure 22 represents this as a function of frequency and distance. It is now possible to compute

the amplitude expected from these phase velocities under the (false) assumption of ray optics. That computed amplitude is seen (Figure 21) to be quite similar to the correct diffraction amplitude. Thus, despite their cross-checking of the amplitude data with the travel-time data, Cleary may not have been seeing ray-optical defocusing at all.

It is of some interest to look for the phase velocity distortion in our long period data. Using the Kermadec earthquake of 20 May 1963, four stations were Fourier analyzed. The phase spectrum was converted to a phase "arrival time" at each frequency, and this was added to the starting time of the window. In plotting, a straight line with a slope of 24.82 km/sec was subtracted from the data and residuals plotted (Figure 23). At the greater distances, the lower frequencies are seen to have slightly lower phase velocities. In general, however, this is a fairly delicate measurement, made more so by the expected variation of phase velocity with distance. Sacks (1967) has attempted most recently to fix the phase velocity by time domain measurements on diffracted waves; his determination of  $24.55 \pm .08$  km/sec. lies within the scatter of our results. Both studies, however, have used long periods. Figure 22 suggests that the true high frequency value might be underestimated by 1 km/sec.

In conclusion, it should be noted that we are reluctant in this paper to engage in modeling of the actual core. This has

been the object of much recent attention. Our objective here is to make available a more correct physical description of the shadowing process and to indicate by examples the types of data analysis which are affected. In general we have reservations about the use of time domain measurements on data which is easily described only in the frequency domain, especially when the measurement being attempted is quite delicate. In fact, it is not clear that even present networks have the usable bandwidth and calibration quality needed to do high resolution studies of the core, even in the frequency domain.

### Acknowledgments

This work was supported by the Air Force Office of Scientific Research under contract AF 49(638) - 1243. The computer facilities were partly supported by National Science Foundation grant GP 579. Digitized data from the Long Range Seismic Measurements network were supplied by the Teledyne Seismic Data Laboratory, Alexandria, Virginia.

#### REFERENCES

- Abramowitz, M., and I.A. Stegun, editors, Handbook of Mathematical Functions, Dover, N.Y., 1965, 1046 pp.
- Alexander, S.S., and R.A. Phinney, A study of the core-mantle boundary using P-waves diffracted by the earth's core. J. Geophys. Research, 71 (24), 5959-5975, 1966.
- Born, M., and E. Wolf, Principles of Optics, Pergamon Press, 1965, 3rd edition, 808 pp.
- Bremmer, H., Terrestrial Radio Waves, Elsevier Publishing Co., Amsterdam, 1949.
- Broome, P.W., Amplitude anomalies at LASA, report LL-7, Teledyne Co. Alexandria, Virginia, 9 August 1967.
- Cleary, J., Analysis of the amplitudes of short-period P-waves recorded by long range seismic measurements stations in the distance range  $30^\circ$  to  $102^\circ$ , J. Geophys. Res., 72, no. 18, 4705-4712, 1967.
- Duwalo, G., and J.A. Jacobs, Effects of a liquid core on the propagation of seismic waves, Can. J. Phys., 37, 109-128, 1956.
- Haskell, Norman A., Crustal reflection of plane P and Sv waves J. Geophys. Res., 67, 4751-4767, 1962.
- Knopoff, L., and F. Gilbert, Diffraction of elastic waves by the core of the earth, Bull. Seism. Soc. Am., 51, no. 1, 35-50, Jan. 1961.

- Nussenzweig, H.M., High-frequency scattering by an impenetrable sphere, Ann. Phys., 34, 23-95, 1965.
- Phinney, R.A., and S.S. Alexander, P Wave diffraction theory and the structure of the core-mantle boundary, J. Geophys. Res., 71, no. 24, 5943-5958, 1966.
- Sacks, S., Diffracted wave studies of the earth's core, 1, amplitudes, core size, and rigidity, J. Geophys. Res., 71, 1173-1182, 1966.
- Sacks, I.S., Diffracted P-wave studies of the earth's core, 2, J. Geophys. Res., 72, no. 10, 2589-2594, 1967.
- Scholte, J.G.J., On seismic waves in a spherical earth, Koninkl. Ned. Meteorol. Inst. Publ., 65, 1956.
- Teng, T L., Attenuation of body waves and the Q structure of the mantle, J. Geophys. Res., 73, no. 6, 2195-2208, 1968.
- Teng, T.L., and Richards, Diffracted P, SV, and SH waves and their shadow-boundary shifts, in press.
- Teng, T L., and F.T. Wu, A two-dimensional ultrasonic model study of compressional and sphere wave diffraction patterns produced by a circular cavity, Bull. Seis. Soc. Am., 58, no. 1, 171-178, 1968.
- Watson, G.N., The diffraction of electric waves by the earth, Proc. Roy. Soc. London, A., 95, 83, 1918.

LIST OF TABLES

- Table 1 Fresnel integral function  $D(\oplus)$ . For use with equations (5) and (6) to construct an approximate theoretical amplitude across the shadow boundary.
- Table 2 Theoretical diffraction amplitude for Model 1, for use in forming data residuals: The arbitrary zero of ordinates is set so that the ray-theoretical amplitude  $1/kR$  is at zero at  $90^\circ$  in the model earth. For this tabulation the epicentral distances are given for the Model 1 parameters and shifted to correspond to a shadow position of  $96.5^\circ$ , for the real earth.  $(\text{Sin}\theta)^{1/2}$  has been taken out.
- Table 3 Brazil earthquake: Source parameters and station distances and azimuths.
- Table 4 Taiwan earthquake: Source parameters and station distances and azimuths.

Table 1

$\Theta$	$D(\Theta)$	$\ln D(\Theta)$	Remarks
	2.000	.697	Asymptotic value
-1.5	2.156	0.768	Illuminated region
-1.4	2.236	.817	
-1.3	2.325	.844	
-1.2	2.341	.850	First maximum
-1.1	2.312	.838	
-1.0	2.244	0.808	
-0.9	2.147	.764	
-0.8	2.028	.707	
-0.7	1.896	.639	
-0.6	1.756	.563	
-0.5	1.615	0.479	
-0.4	1.476	.388	
-0.3	1.344	.296	
-0.2	1.220	.199	
-0.1	1.105	.099	Illuminated region
0.	1.000	0.000	Geometrical shadow position
0.1	.905	-0.099	Shadow region
0.2	.820	- .199	
0.3	.743	- .297	

0.3	.743	- .297	
0.4	.676	- .392	
0.5	0.616	-0.485	
0.6	.563	- .575	
0.7	.516	- .662	
0.8	.474	- .746	
0.9	.438	- .826	
1.0	0.4053	-0.902	Deep shadow entries at
1.1111	.3736	- .985	reciprocal integers
1.2500	.3394	-1.080	
1.4285	.3026	-1.196	
1.6667	.2634	-1.333	
2.0000	0.2221	-1.504	
2.5000	.1790	-1.715	
3.3333	.1348	-2.004	
5.0000	.0900	-2.408	
10.0000	.0450	-3.101	Shadow region

Table 2

Model 1 Distance $\theta_s = 113.5^\circ$	Shifted Distance for real Earth $\theta_s = 96.5^\circ$	Natural log of Diffraction amplitude						
		Ka=32 f=.02	48 .03	64 .04	80 .05	96 .06	112 .07	128 .08
90°	73°	0.023	-0.092	-0.094	0.018	0.104	0.092	-0.011
92	75	.037	- .049	- .116	- .090	- .003	.067	+0.078
94	77	.032	- .013	- .080	- .122	- .106	- .047	.014
96	79	.010	+ .000	- .038	- .085	- .119	- .124	- .099
98	81	- .030	- .013	- .021	- .044	- .074	- .103	- .124
100°	83°	-0.083	-0.051	-0.037	-0.035	-0.042	-0.057	-0.076
102	85	- .149	- .111	- .085	- .066	- .054	- .049	-0.049
104	87	- .224	- .189	- .159	- .134	- .112	- .094	- .080
106	89	- .308	- .281	- .256	- .231	- .208	- .187	- .169
108	91	- .397	- .384	- .368	- .352	- .334	- .318	- .302
110°	93°	-0.492	-0.495	-0.493	-0.489	-0.482	-0.474	-0.466
112	95	- .590	- .612	- .626	- .636	- .643	- .648	- .650
114	97	- .691	- .732	- .764	- .790	- .811	- .829	- .843
116	99	- .793	- .855	- .905	- .947	- .981	-1.012	-1.038
118	101	- .895	- .977	-1.045	-1.102	-1.150	-1.192	-1.230
120°	103°	-0.998	-1.100	-1.184	-1.255	-1.315	-1.369	-1.419
122	105	-1.099	-1.220	-1.320	-1.403	-1.474	-1.540	-1.599
124	107	-1.200	-1.339	-1.453	-1.547	-1.629	-1.705	-1.772
126	109	-1.300	-1.456	-1.582	-1.687	-1.780	-1.864	-1.936
128	111	-1.398	-1.570	-1.707	-1.823	-1.925	-2.016	-2.095

130°	113°	-1.495	-1.682	-1.829	-1.955	-2.066	-2.163	-2.251
132	115	-1.590	-1.791	-1.948	-2.084	-2.203	-2.305	-2.402
134	117	-1.684	-1.898	-2.065	-2.211	-2.335	-2.447	-2.550
136	119	-1.777	-2.003	-2.180	-2.335	-2.466	-2.586	-2.694
138	121	-1.869	-2.106	-2.294	-2.457	-2.595	-2.723	-2.835
140°	123°	-1.959	-2.208	-2.406	-2.576	-2.724	-2.857	-2.977
142	125	-2.049	-2.309	-2.517	-2.695	-2.852	-2.988	-3.118
144	127	-2.137	-2.409	-2.628	-2.812	-2.978	-3.119	-3.258
146	129	-2.225	-2.508	-2.737	-2.930	-3.103	-3.251	-3.396
148	131	-2.312	-2.607	-2.845	-3.048	-3.226	-3.385	-2.532

Table 3

Station	Distance	Azimuth
PTO	76.4°	43.9°
TOL	79.0	46.4
STU	90.6	40.7
AQU	92.3	47.6
KON	93.2	47.6
NOR	93.9	7.1
NUR	100.8	30.1
KEV	101.3	20.5
IST	103.8	50.0
HLW	105.5	61.5
NAI	107.5	94.6
SHI	123.7	60.7
QUE	135.8	55.8
NDI	144.7	52.6
SHL	157.1	42.8

Time: 9 November 1963, 21h, 15m, 30.4s

Location: W. Brazil, 9.000S 71.500W

Magnitude: 6.8, Depth: 600km.

Table 4

Station	Distance	Azimuth	
WINV	94.5	40.5	LRSM Stations used in Taiwan-North America analysis.
TFCL	96.7	46.6	
KNUT	100.1	41.5	
CPCL	100.6	46.8	
FSAZ	102.3	42.2	
WNSD	102.3	30.0	
DRCO	102.7	38.4	
SEMN	103.7	26.0	
HBOK	109.2	34.5	
SSTX	111.2	40.4	
GVTX	112.0	34.7	
MPAR	112.5	30.8	
BLWV	114.3	20.0	
MMTN	114.9	24.4	
CCG	78.5	1.0	USCGS World-Wide Stations used in Taiwan-North America analysis.
BKS	93.7	45.4	
GOL	102.4	35.4	
MNN	103.9	24.8	
TUC	104.4	44.0	
MDS	106.4	23.5	

LUB	108.8	37.5
AAM	109.5	19.7
FLO	110.2	26.3
DAL	112.1	34.5
WES	112.3	10.5
GEO	114.5	16.1
BLA	115.1	19.5
SHA	118.1	29.1
BEC	123.1	6.6
CAR	144.2	14.7
TRN	144.9	5.5
QUI	148.9	41.7
COP	80.3	327.2
ATU	81.3	307.7
STU	85.5	322.2
AQU	86.3	315.2
VAL	93.1	333.0
MAL	100.8	318.7
BUL	100.8	253.0
PRE	103.3	248.0

Stations used in Taiwan-Europe  
analysis.

Time: 13 Feb. 1963, 8h, 50m, 2.2s

Location: Taiwan, 24.500N, 121.800E

Magnitude: 7.2                      Depth: shallow

### Figure Captions

1. "Mixed" core boundary. Maps of the function  $\text{Re}(\ln f)$ , where  $f$  is the integrand of equation (3): Top, for  $\theta = 105^\circ$  (illuminated zone) and bottom, for  $130^\circ$  (shadow zone), at  $ka = 200$ . Dashed line is the integration path, which is steepest descent along the two end segments, and passes between the saddle points when  $\theta = 105^\circ$ . At  $130^\circ$ , the two saddle points have coalesced in the neighborhood of the first pole, but the original contour is used for integration.
2. Natural logarithm of diffraction amplitude for "model 1". Straight lines (P) in shadow zone give amplitude based on the residue at the first pole. Lines (1/kR) in illuminated zone give ray-theoretical amplitude of the incident wave.
3. Geometry for calculation of first Fresnel zone.
4. Scaling of characteristic features of diffraction pattern with frequency. Points are obtained by inspection of Figure 2, and lines are drawn with a slope of  $-1/2$ . The central line is a plot of equation (4).
5. Diffraction amplitude estimated by Sacks for periods of 25, 2.5, and 0.7 seconds. The curves are our theoretical amplitudes for these periods (model 1) with amplitude and distance adjustments as described in the text.
6. Natural logarithm of diffraction amplitude for a "mixed" core.
7. Natural logarithm of diffraction amplitude for a "hollow" core.

Figure Captions Continued

8. Comparison of diffraction amplitudes for "hollow" (H), "mixed" (M), "rigid" (R) and "model 1" (1) cores, at  $ka = 200$ .
9. Comparison of exact (dashed) diffraction amplitudes with those given by the Fresnel integral, for an opaque screen, at  $ka = 200, 600$ . The lines a and b show the respective ray-theoretical amplitudes.
10. Brazil earthquake of 9 November 1963: Plot of stations used in the amplitude study.
11. Brazil earthquake of 9 November 1963: Representative time signals and their amplitude spectra.
12. Brazil earthquake of 9 November 1963: Spectral amplitude residuals with respect to the Model 1 theoretical diffraction amplitude, for a shadow at  $96.5^\circ$ . Ordinate units are in natural logarithms, or about 8 db per unit. Solid dots represent points used in determining the deep shadow decay (Fig. 13).
13. Brazil earthquake of 9 November 1963: Spatial decay in deep shadow normalized by  $(ka)^{1/3}$ . Error brackets give the formal standard deviation of a least square fit to the data. Dashed curve gives the theoretical behavior of a Model 1 earth.
14. Taiwan earthquake of 13 February 1963: Plot of stations used in the amplitude study, for azimuths to North America.
15. Taiwan earthquake of 13 February 1963: Representative time

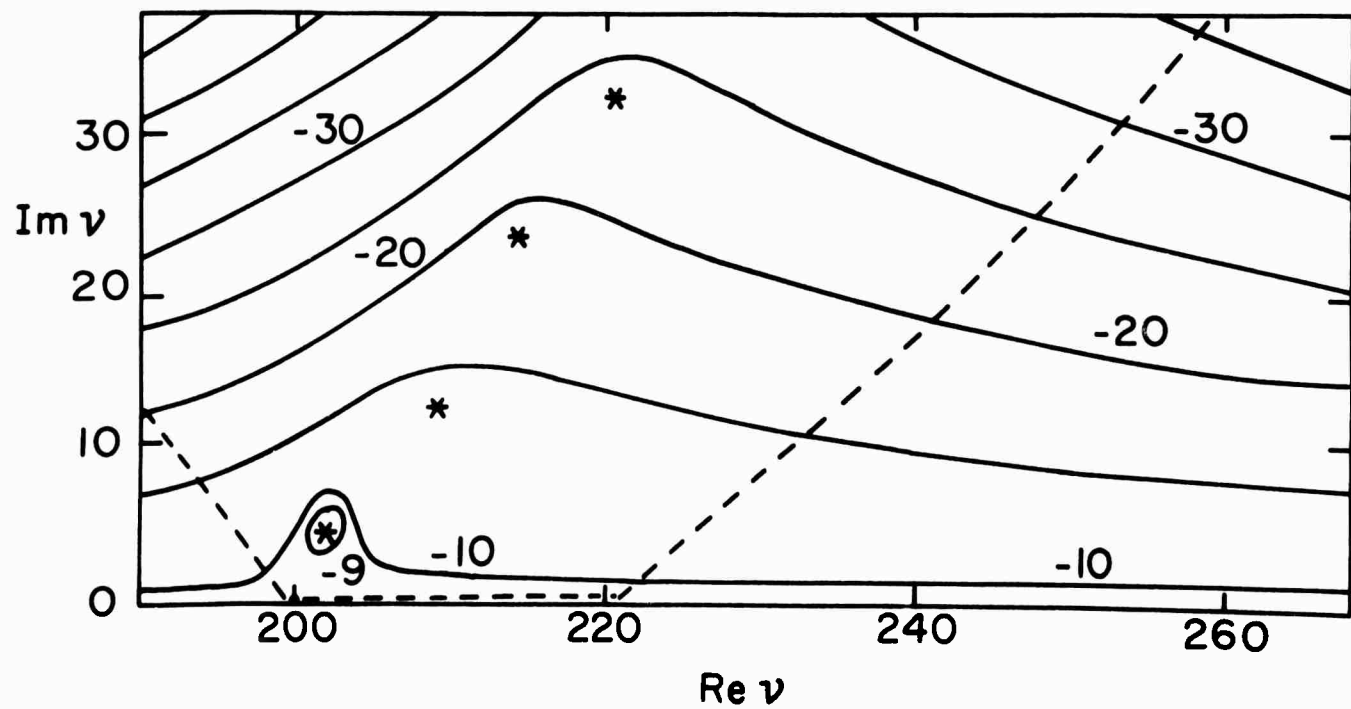
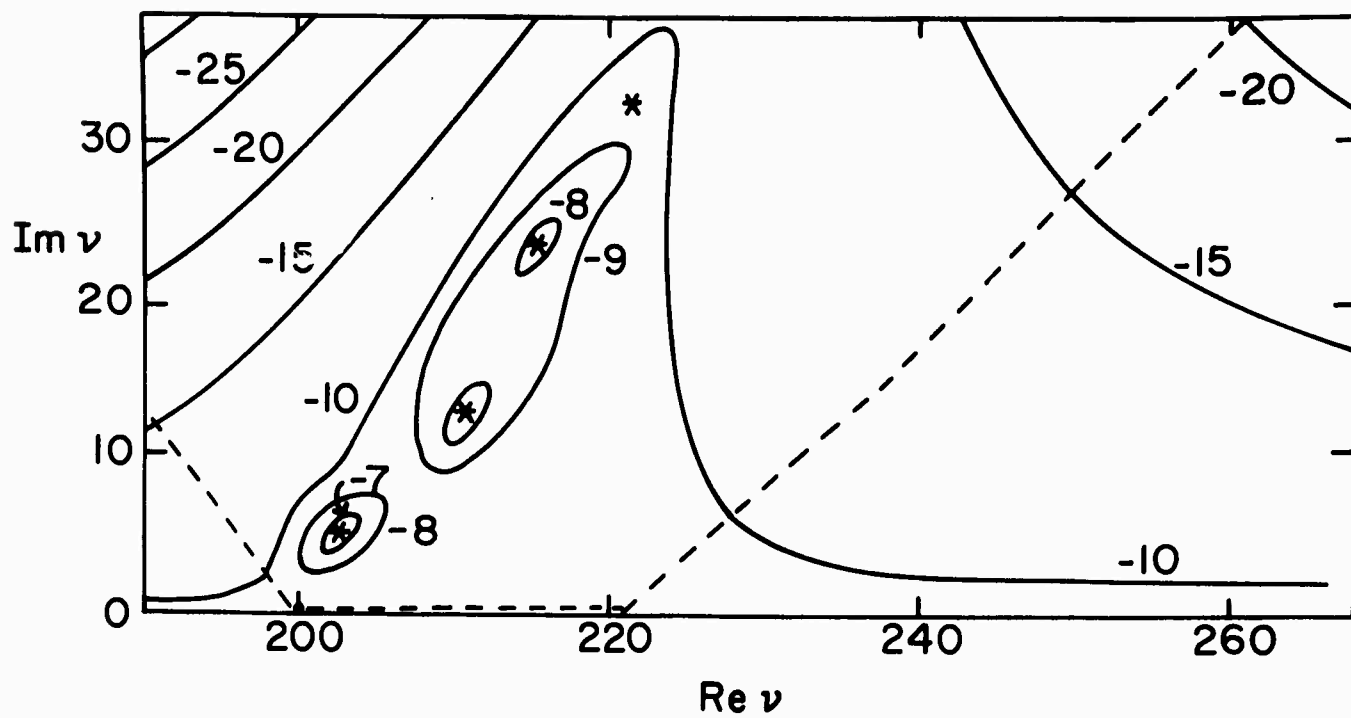
Figure Captions Continued

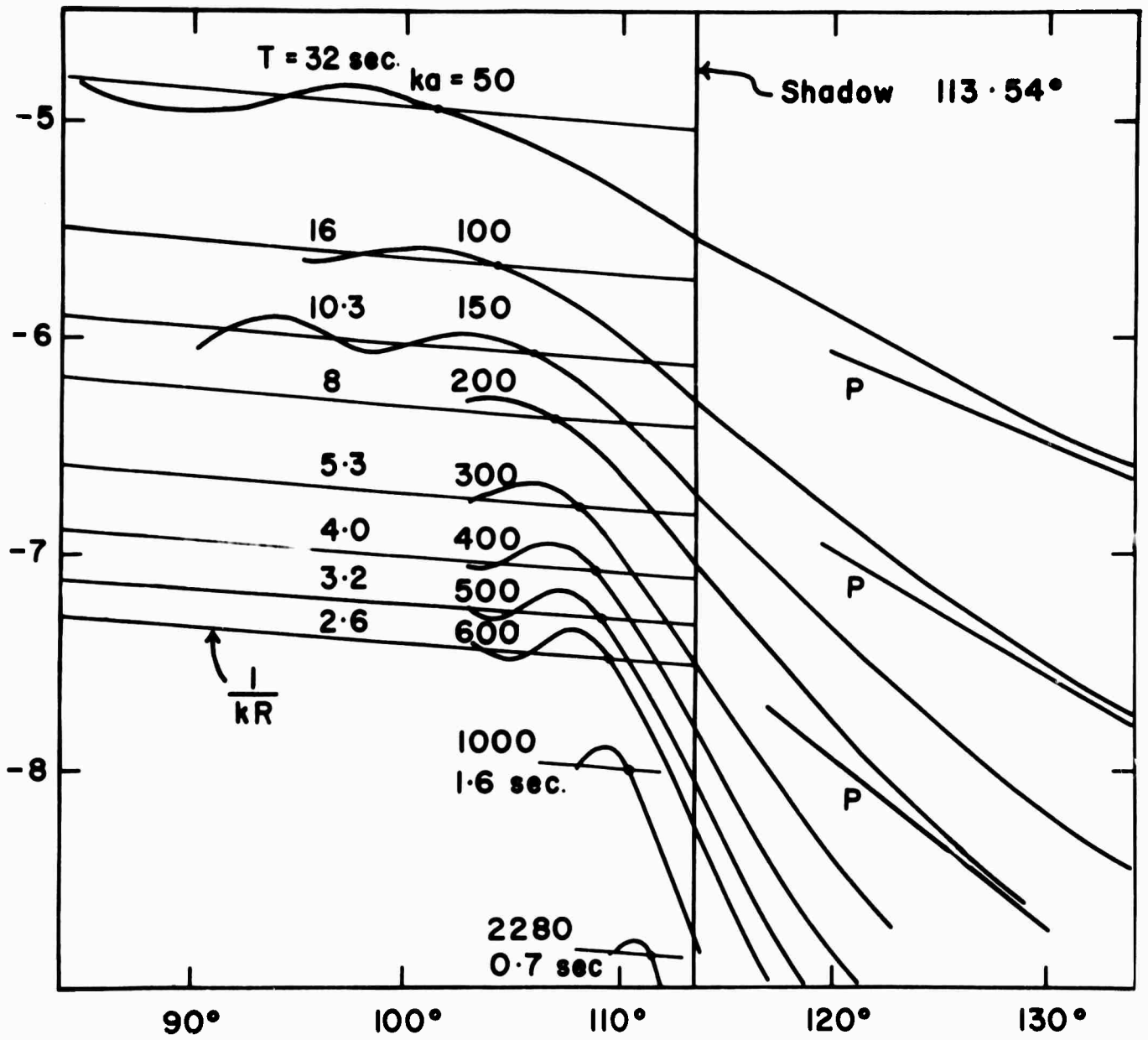
- signals and amplitude spectra; for azimuths to North America. Ordinates are plotted to a scale consistent with that used in Figure 11, except for CCG ( $\times 1/5$ ).
16. Taiwan earthquake of 13 February 1963: Spectral amplitude residuals for azimuths to North America, plotted with the same conventions as in Figure 12.
  17. Taiwan earthquake of 13 February 1963: Spatial decay for azimuths to North America, plotted with the same conventions as in Figure 13.
  18. Taiwan earthquake of 13 February 1963: Plot of stations used in the amplitude study, for azimuths to Europe.
  19. Taiwan earthquake of 13 February 1963: Representative time signals and amplitude spectra, for azimuths to Europe. Spectral ordinates are consistent with Figures 11 and 15; time signal ordinates are consistent with a scaling of  $1/10$ .
  20. Taiwan earthquake of 13 February 1963: Spectral amplitude residuals for azimuths to Europe, plotted with the same conventions as in Figure 12.
  21. Comparison of Cleary and Hales amplitudes with diffraction theory. "Optical" curve is computed from the phase distortion of diffraction theory under ray-optic assumptions.
  22. Analysis of apparent velocity...Model 1. Phase velocity of signal as a function of distance and frequency. Left hand

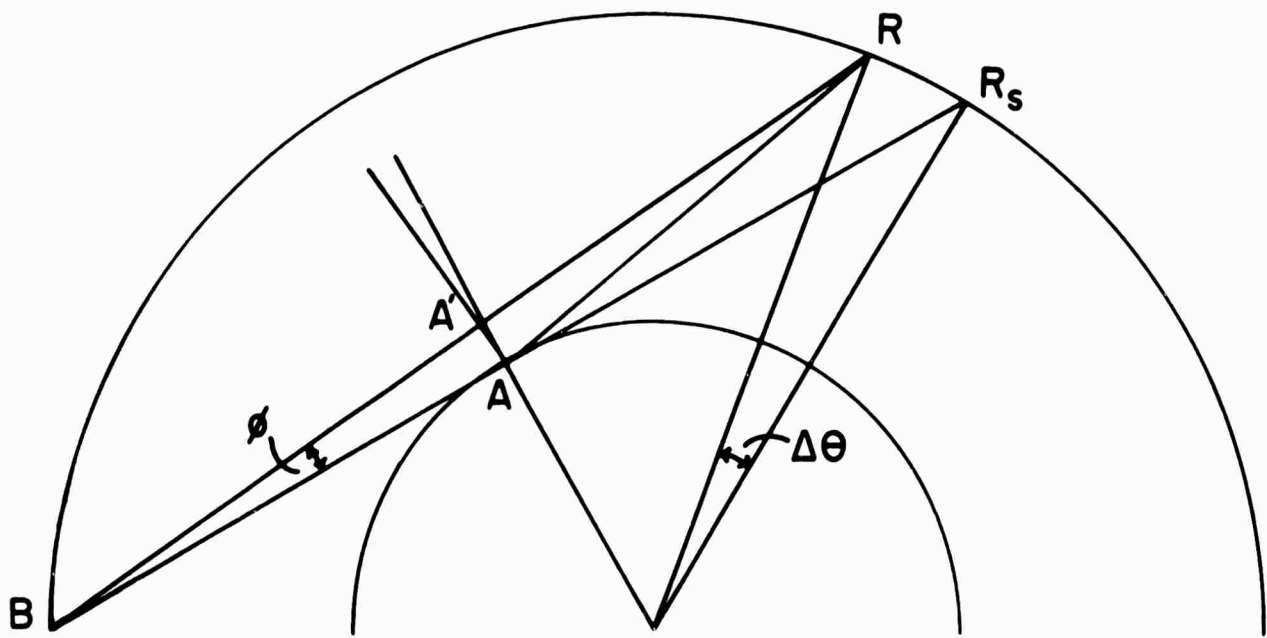
Figure Captions Continued

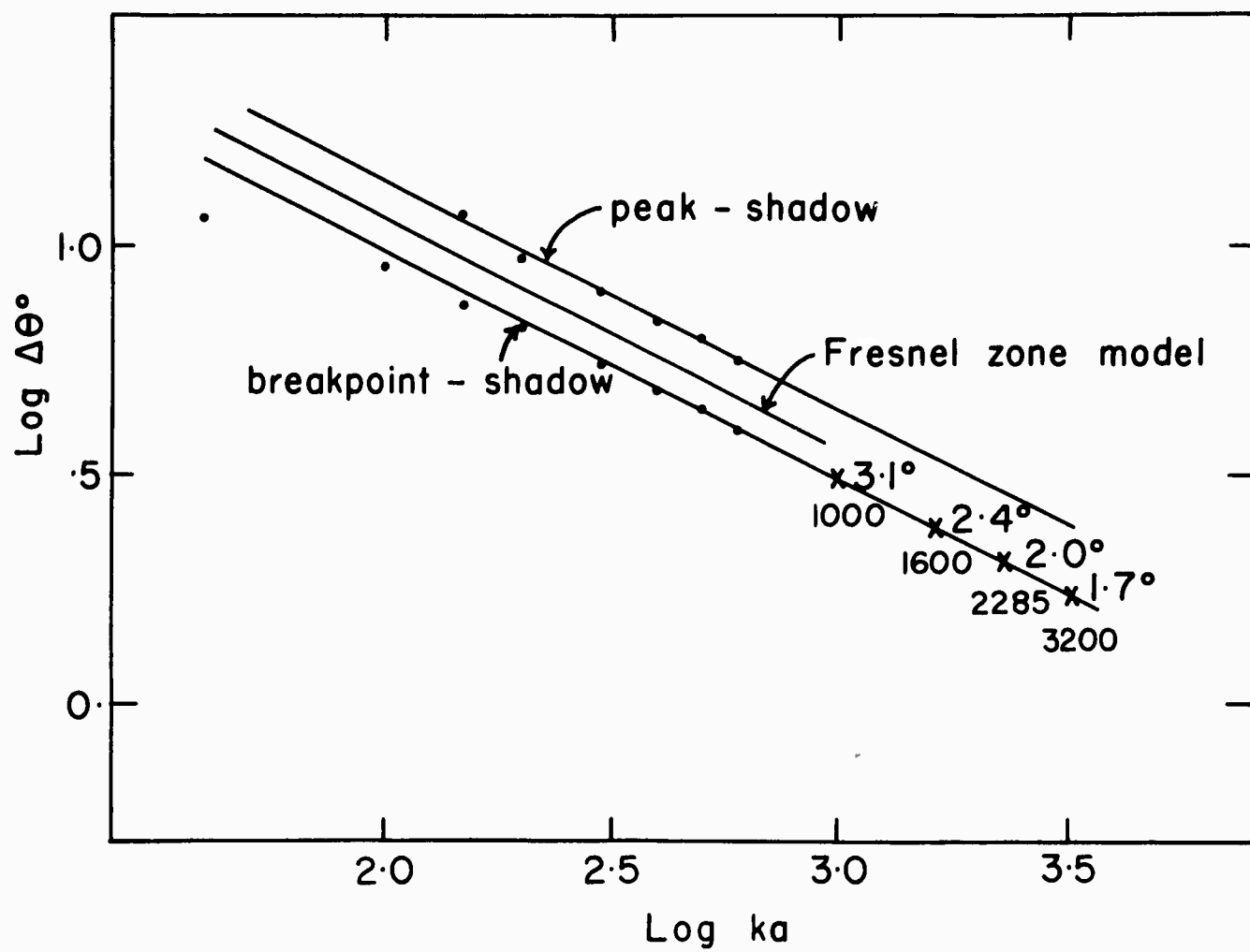
ordinate is phase velocity reduced to base of mantle.

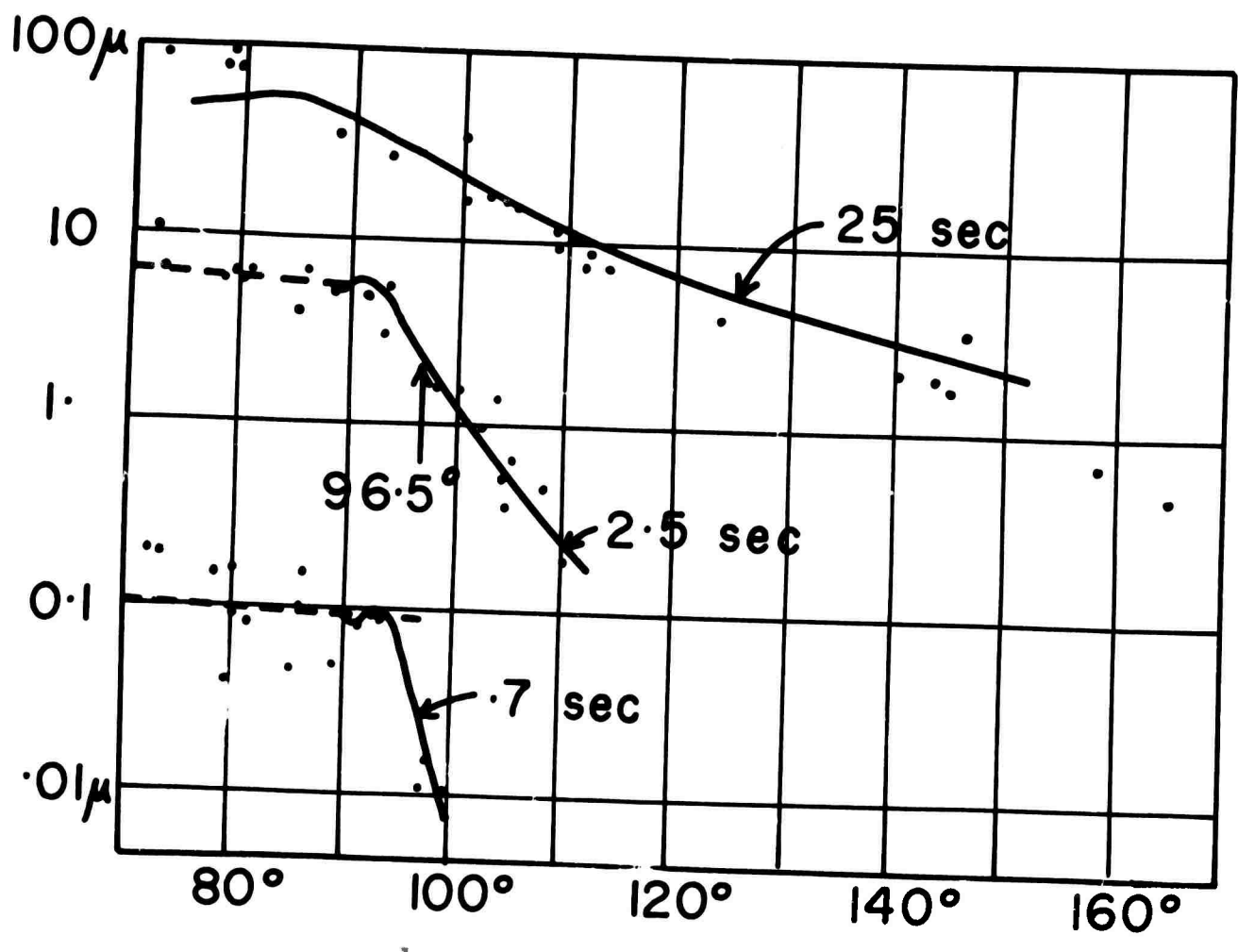
23. Kermadec earthquake of 20 May 1963: Comparison of residual phase arrival times for three frequencies.

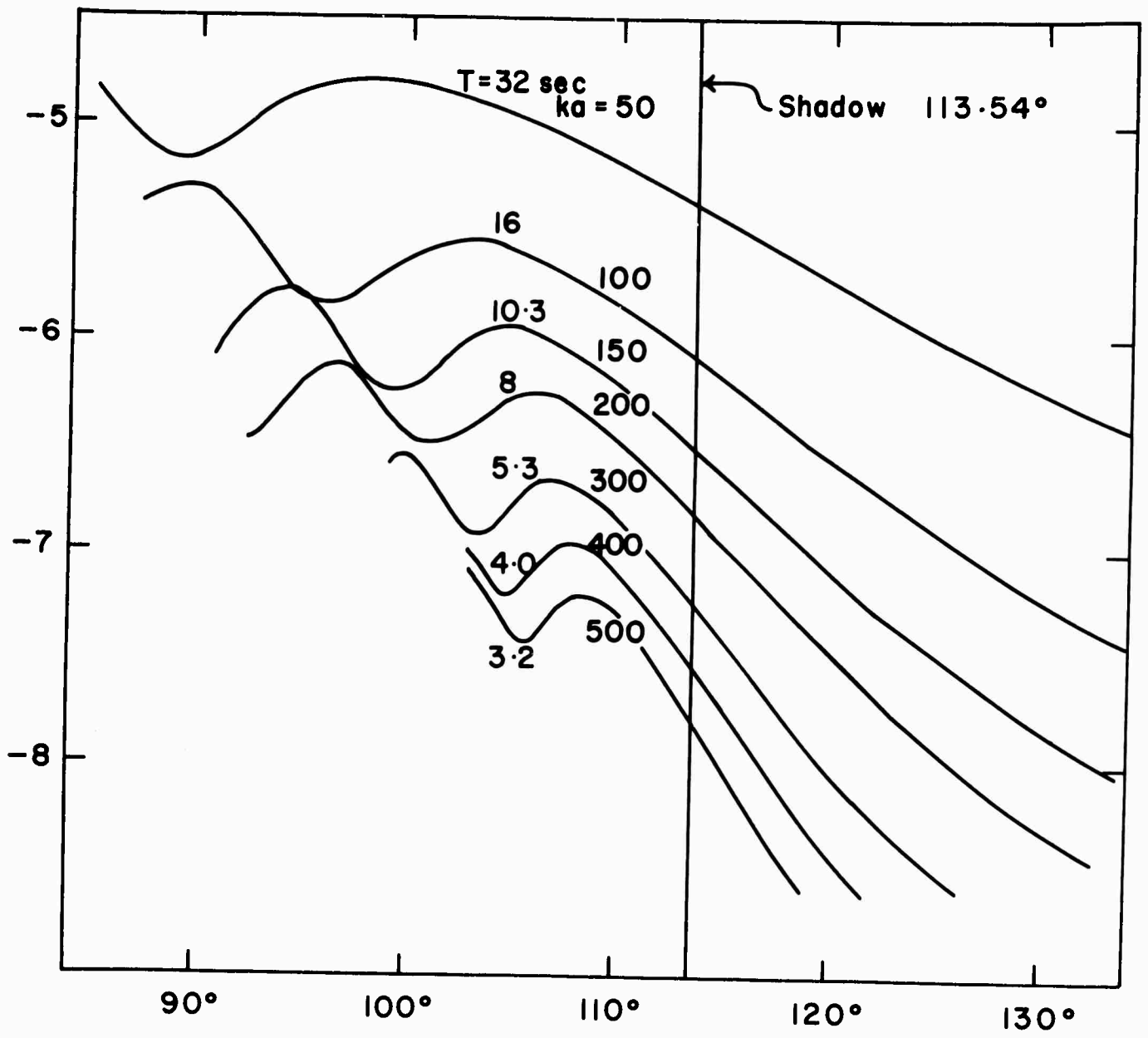


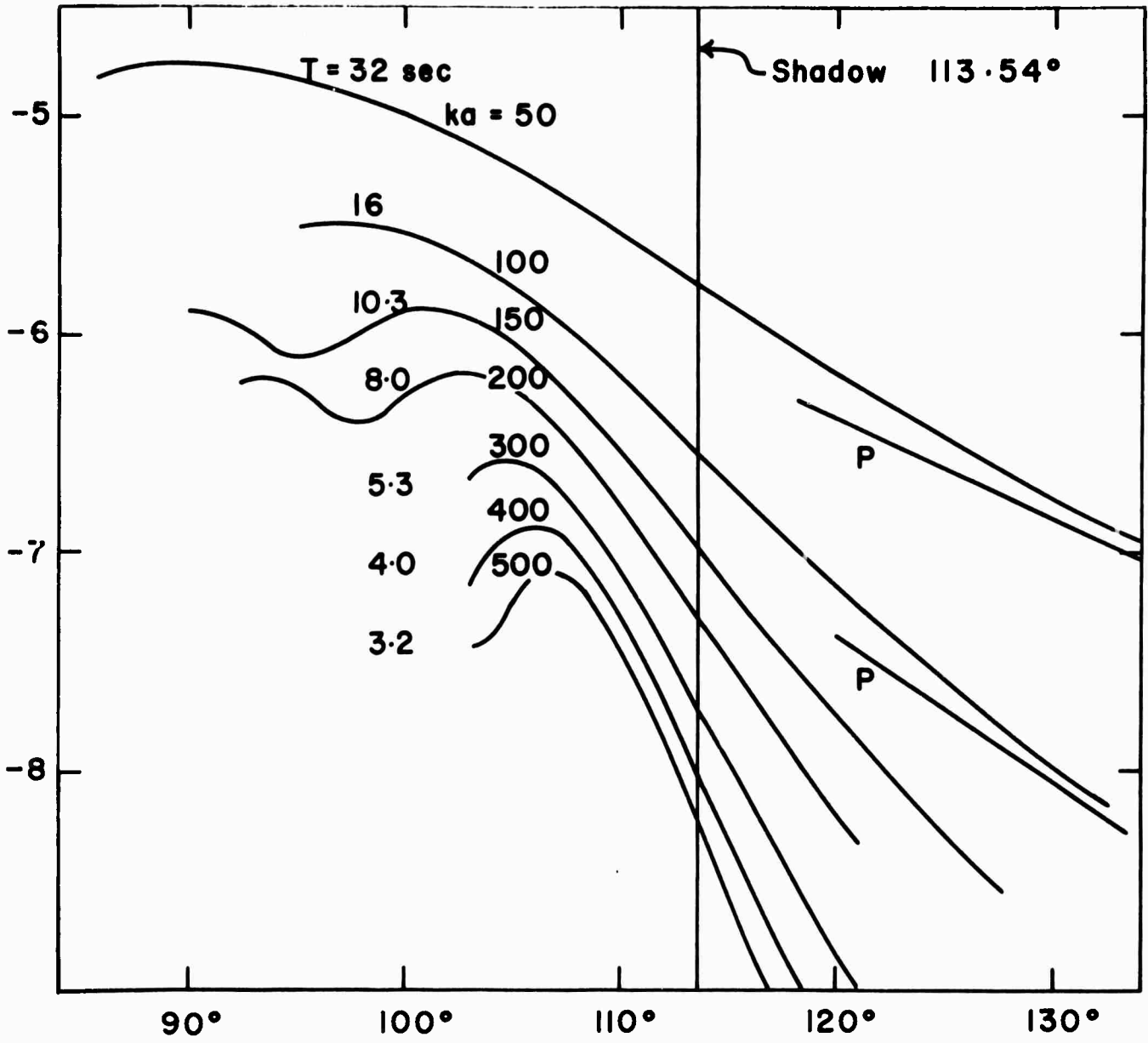


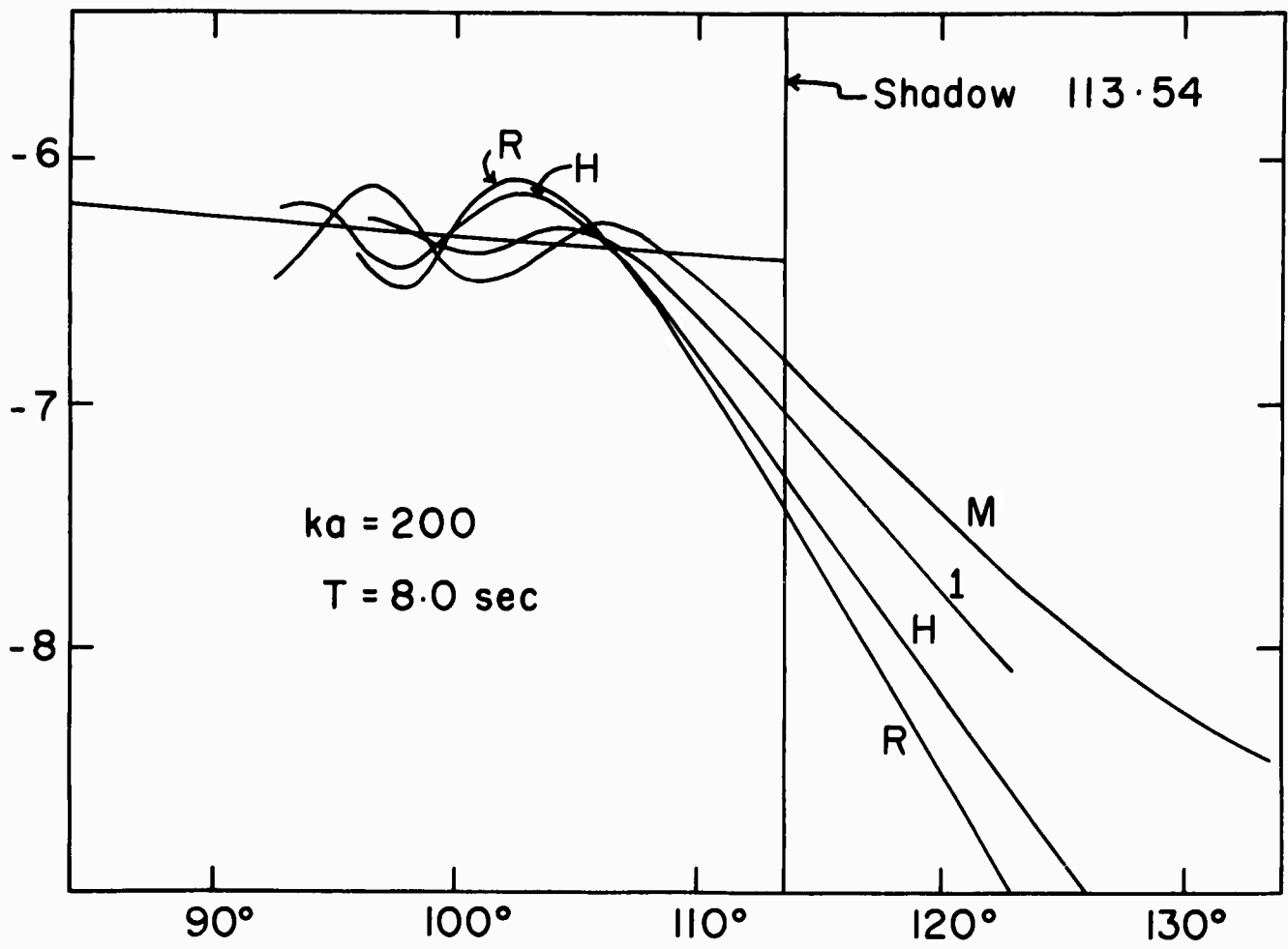


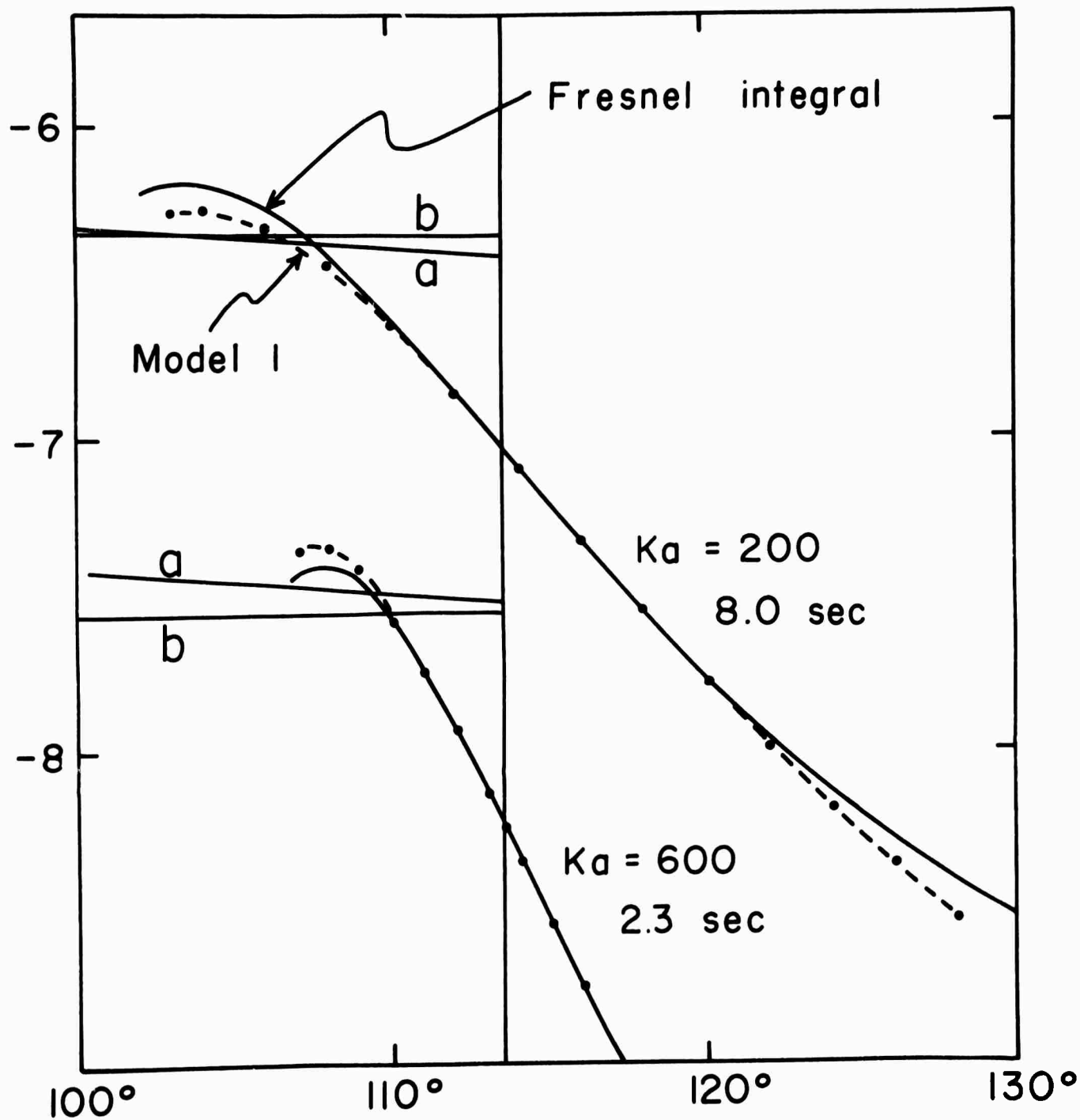




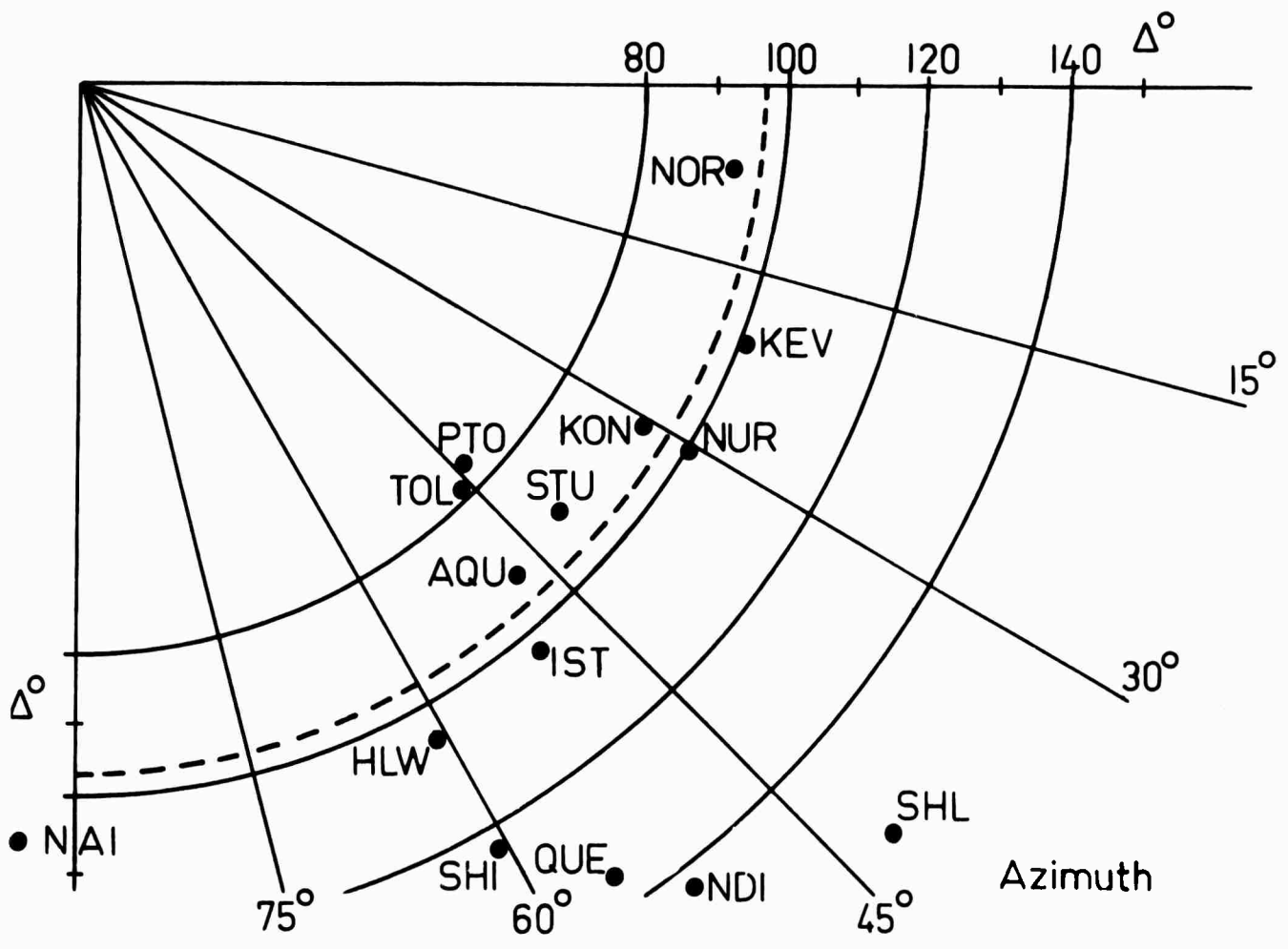




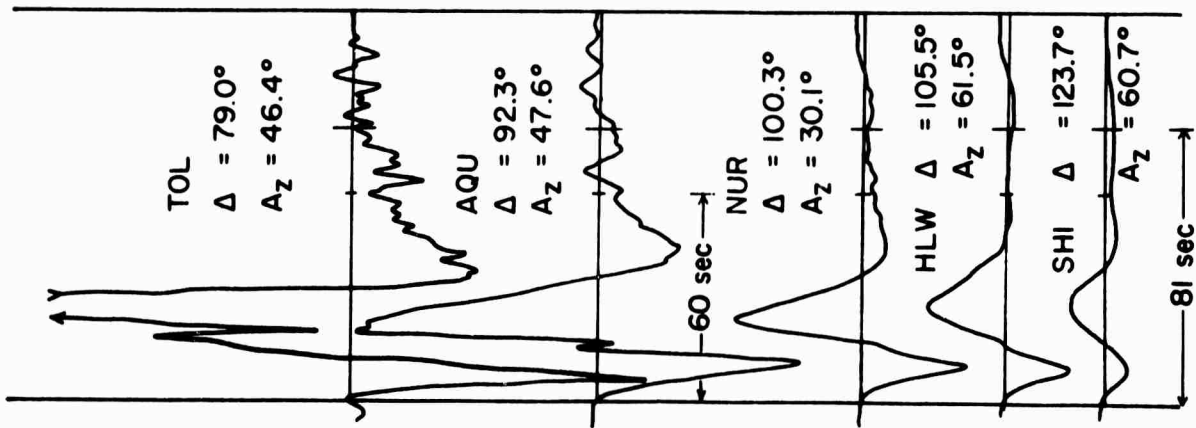
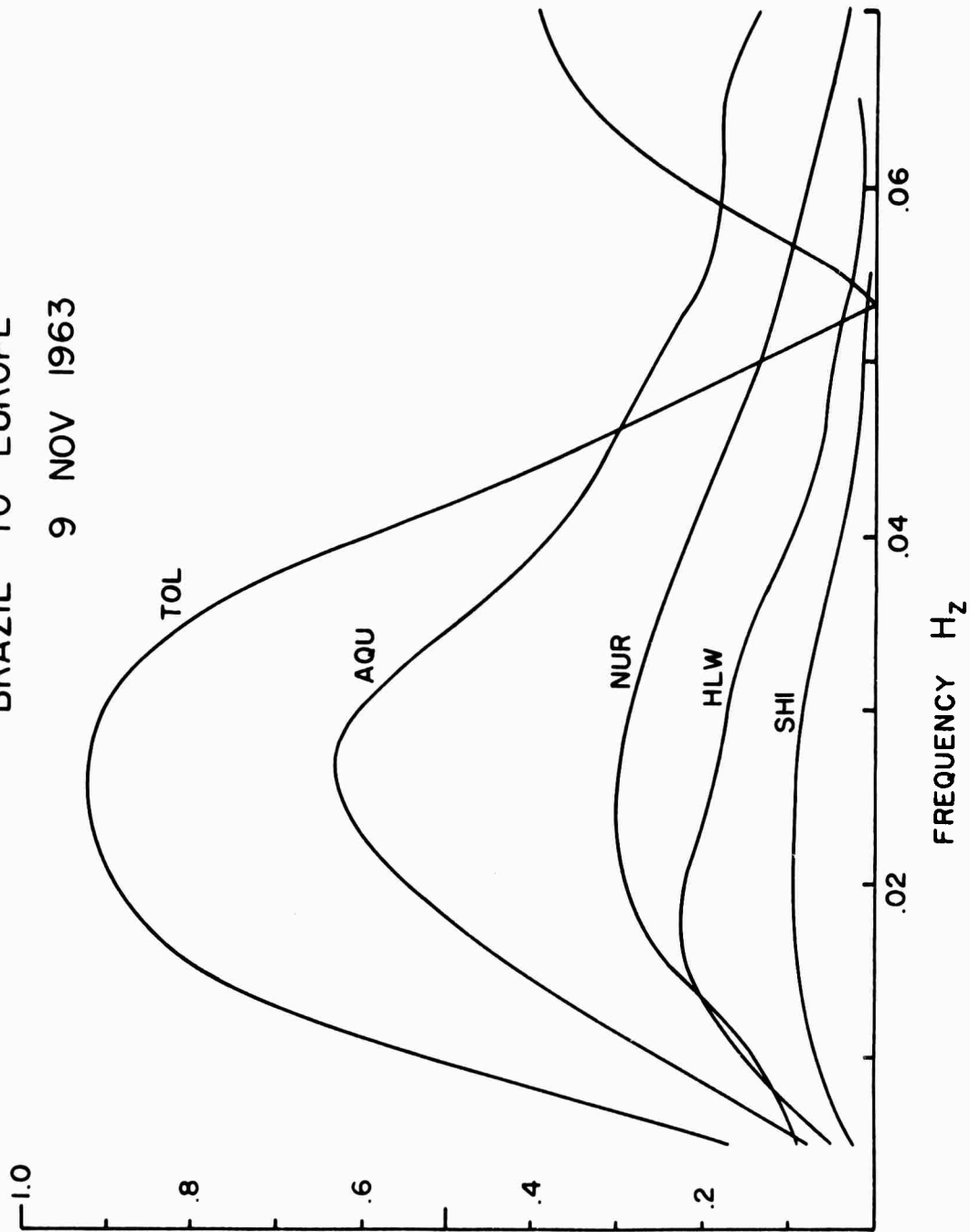


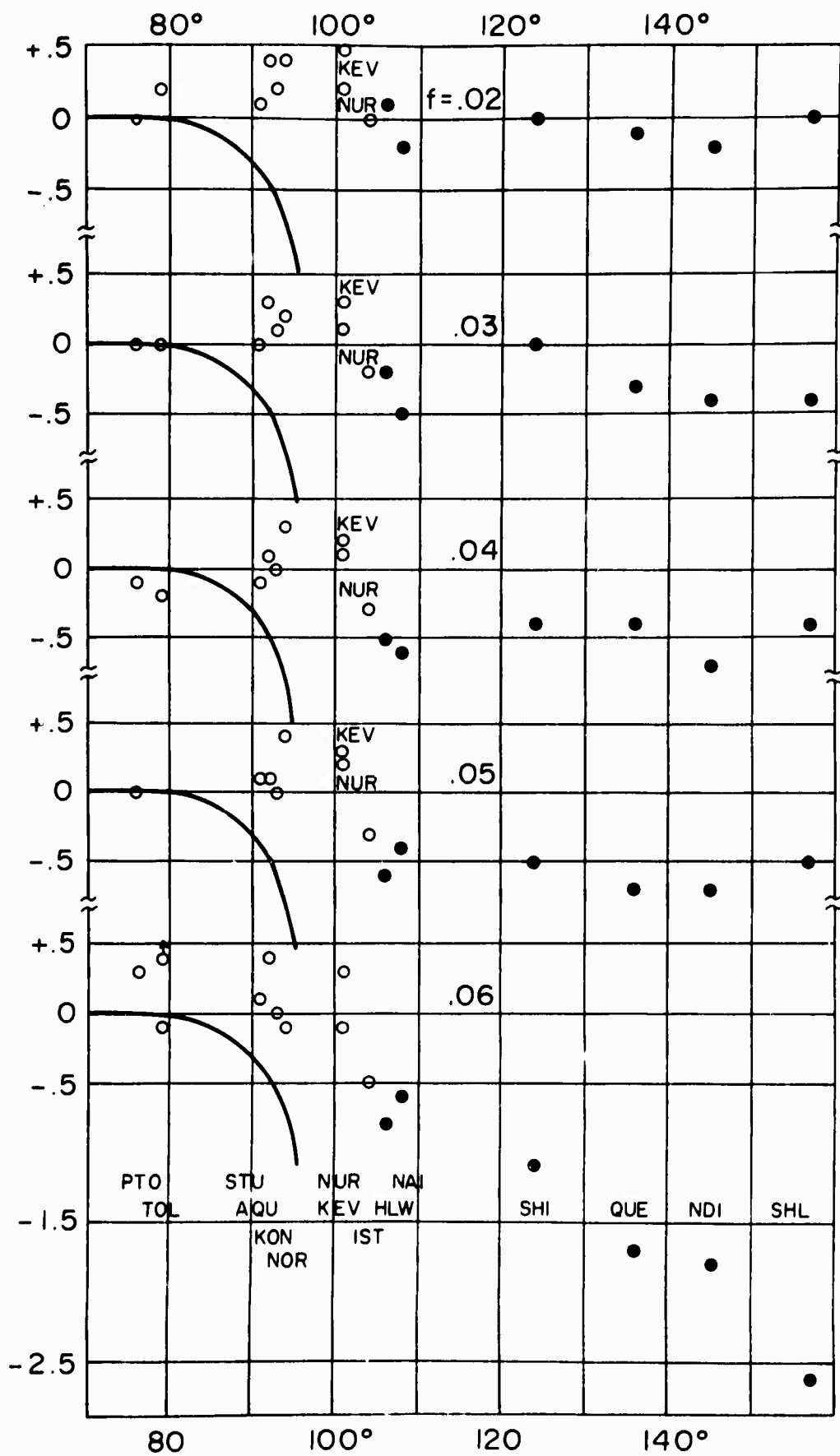


# BRAZIL TO EUROPE 9 NOV 1963

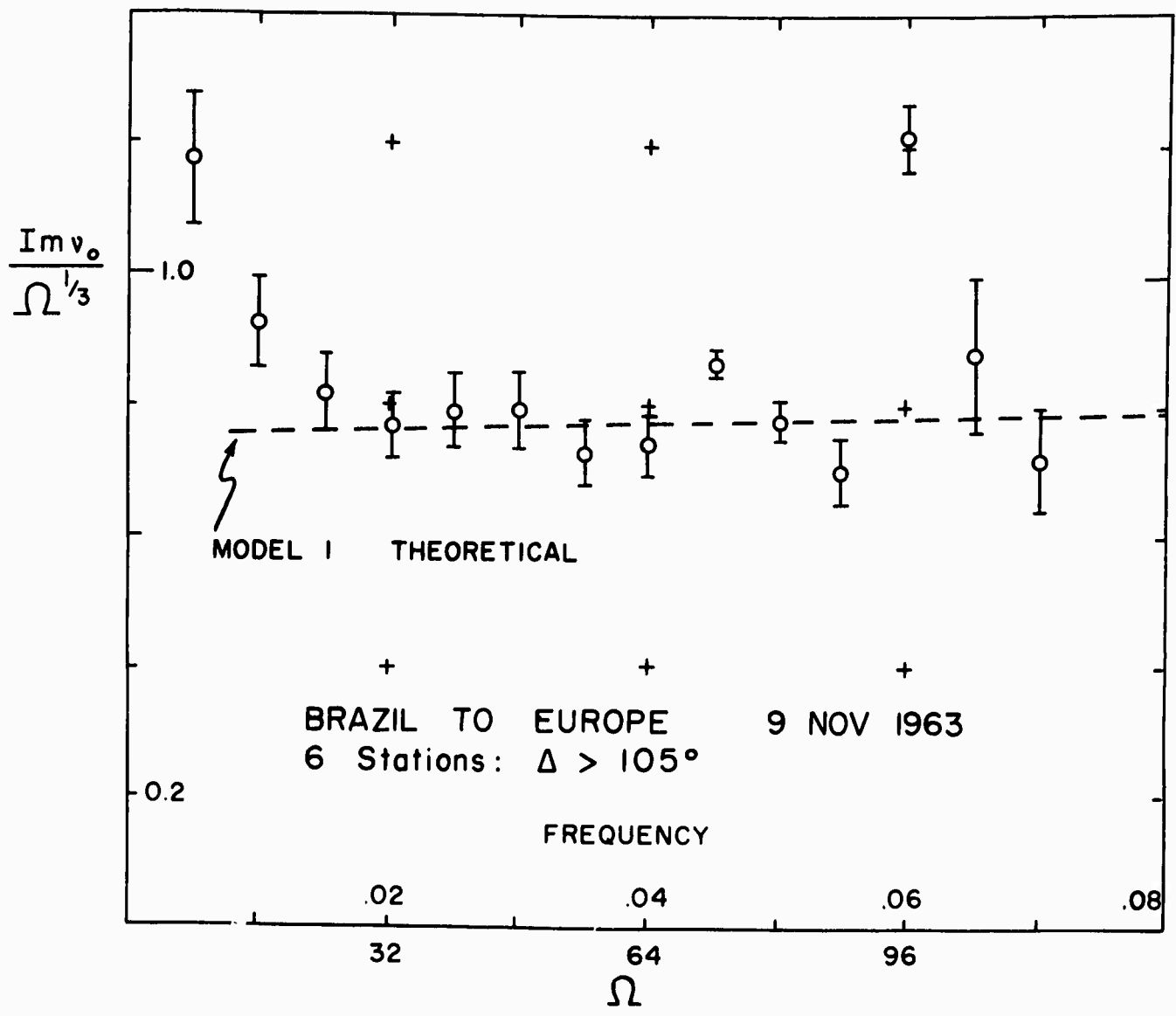


BRAZIL TO EUROPE  
9 NOV 1963

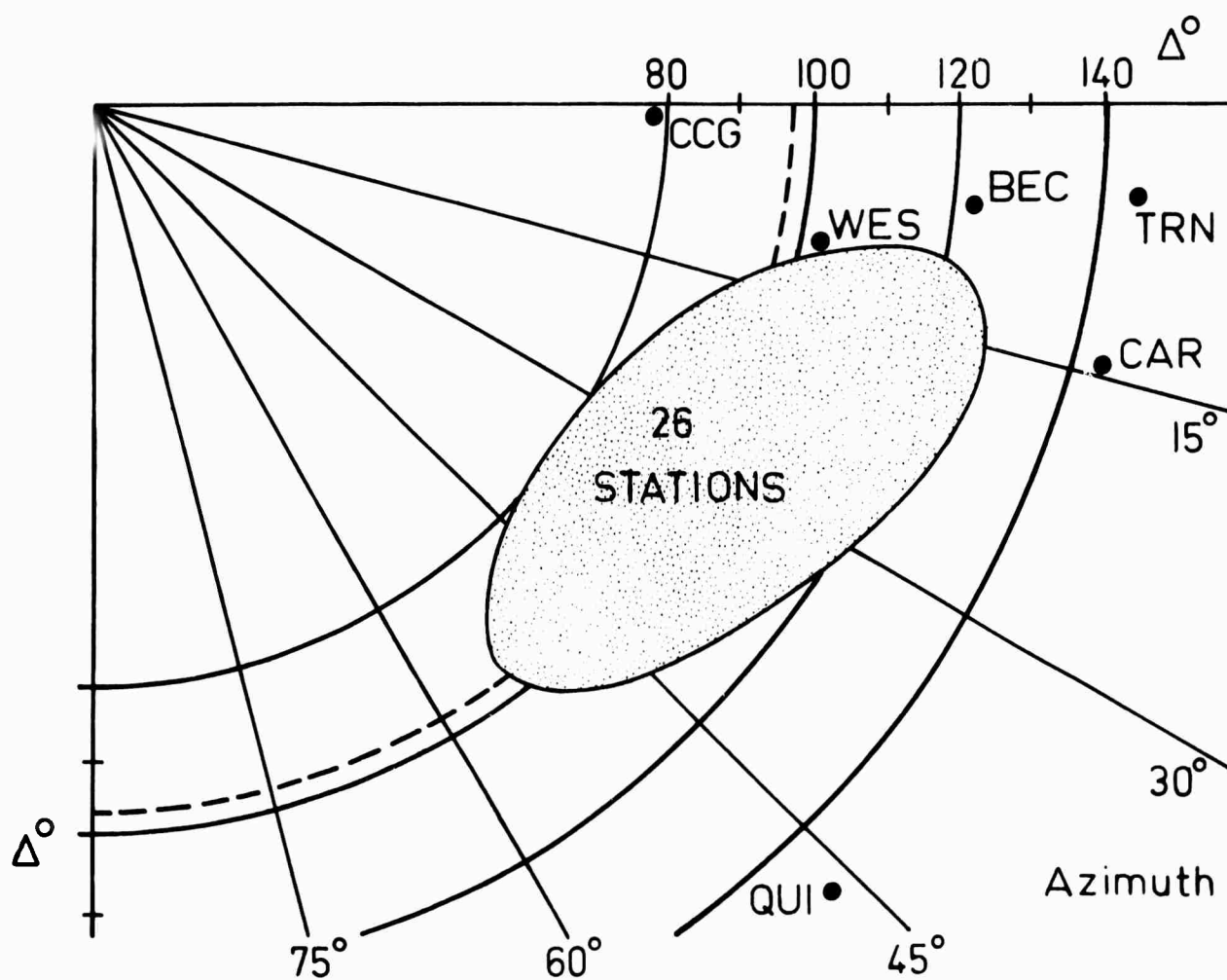




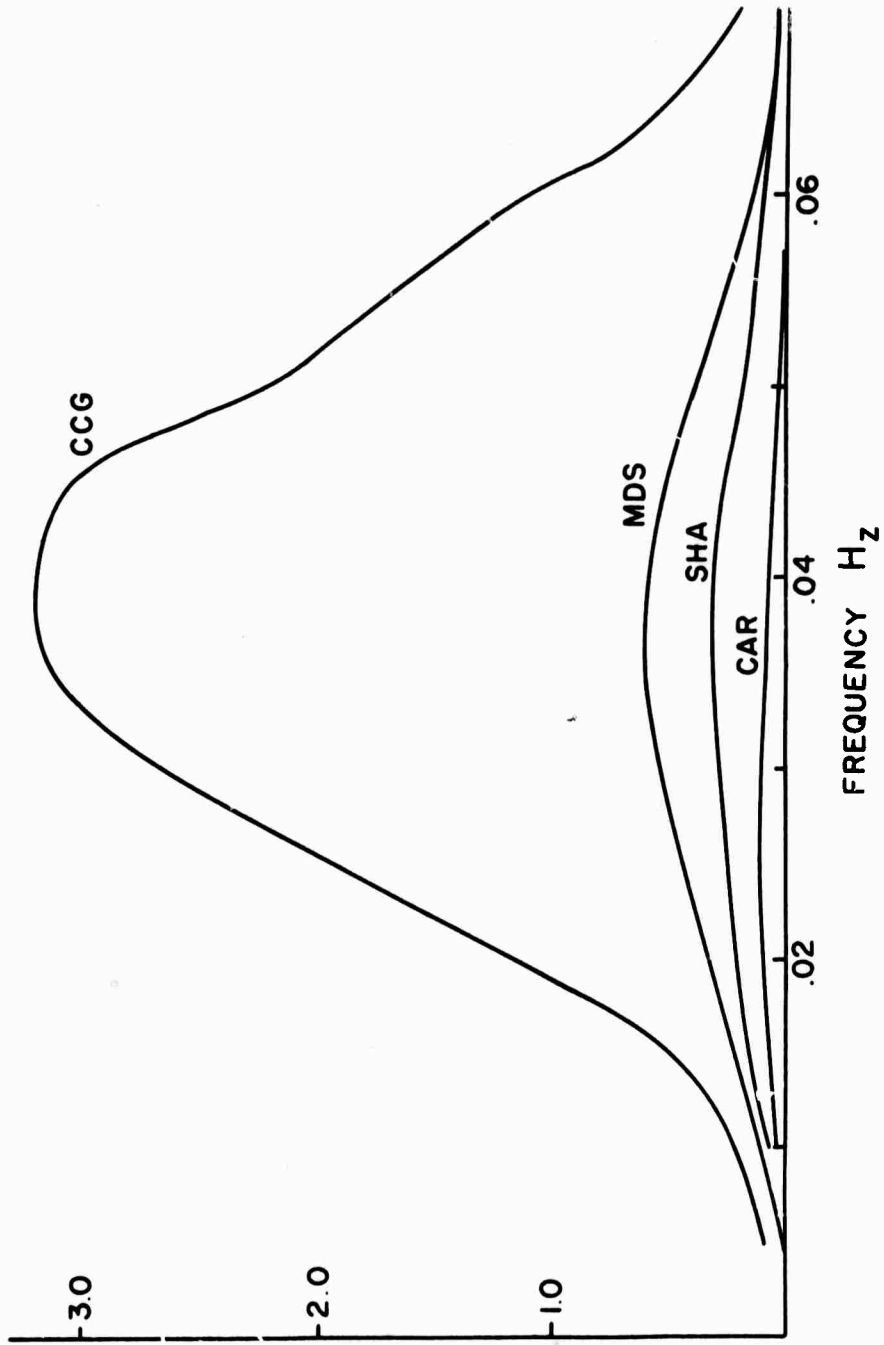
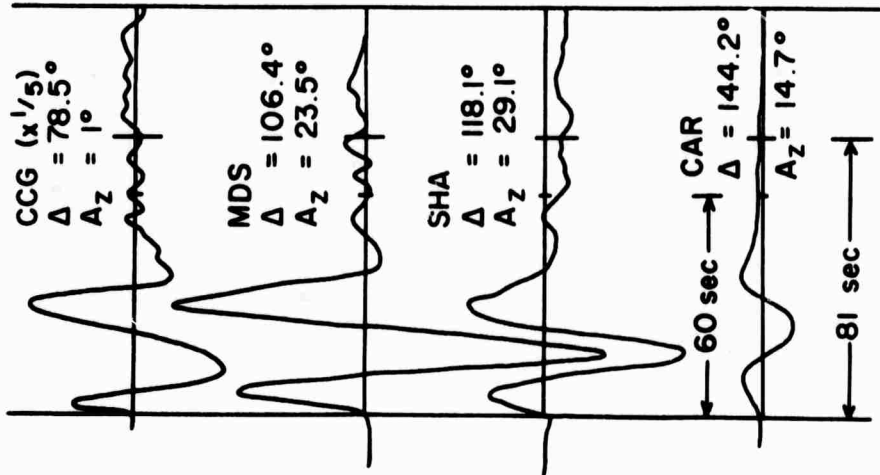
BRAZIL TO EUROPE 9 NOV 1963  
P DIFFRACTION RESIDUALS

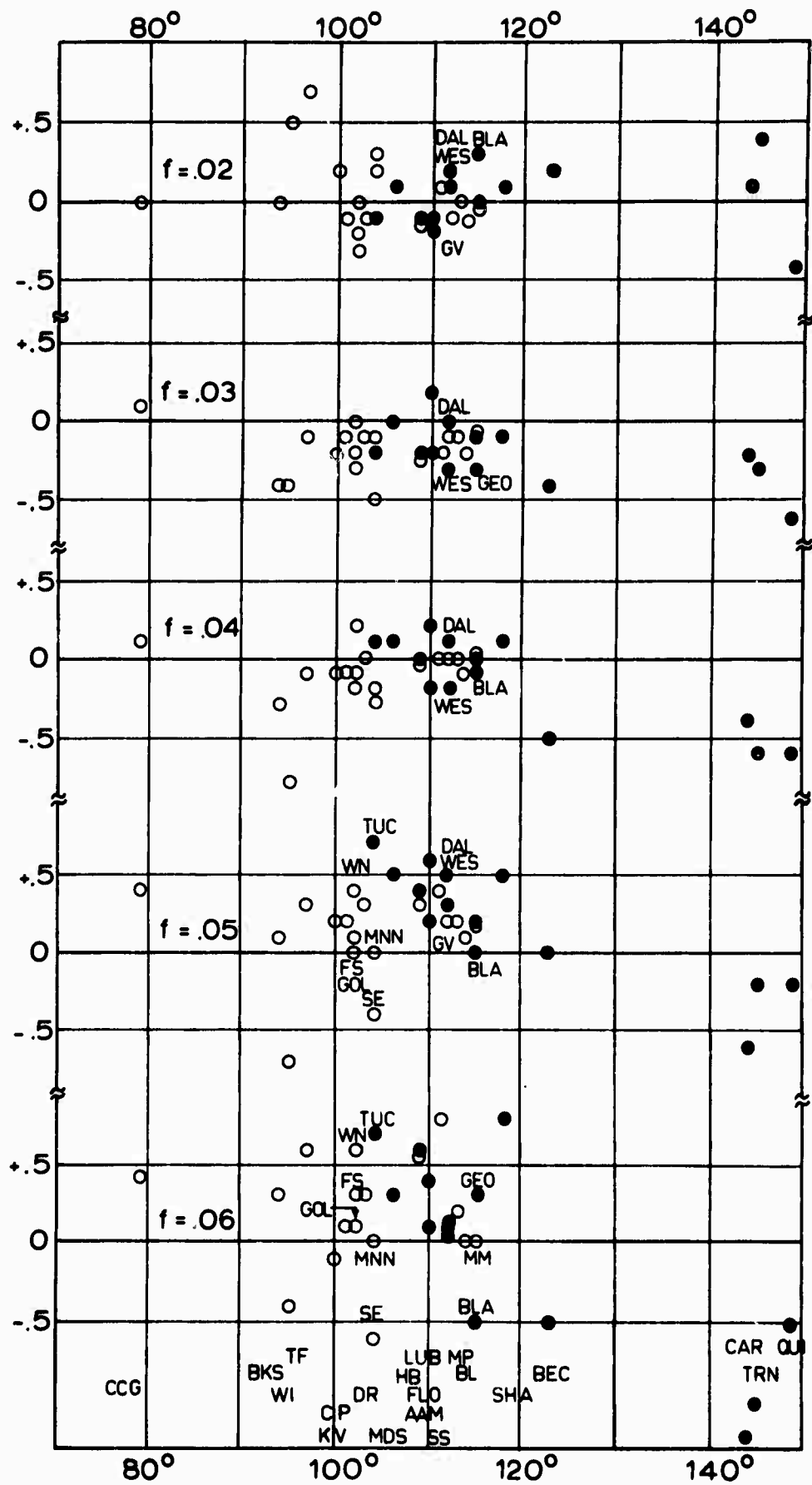


# TAIWAN TO N. AMERICA 13 FEB 1963

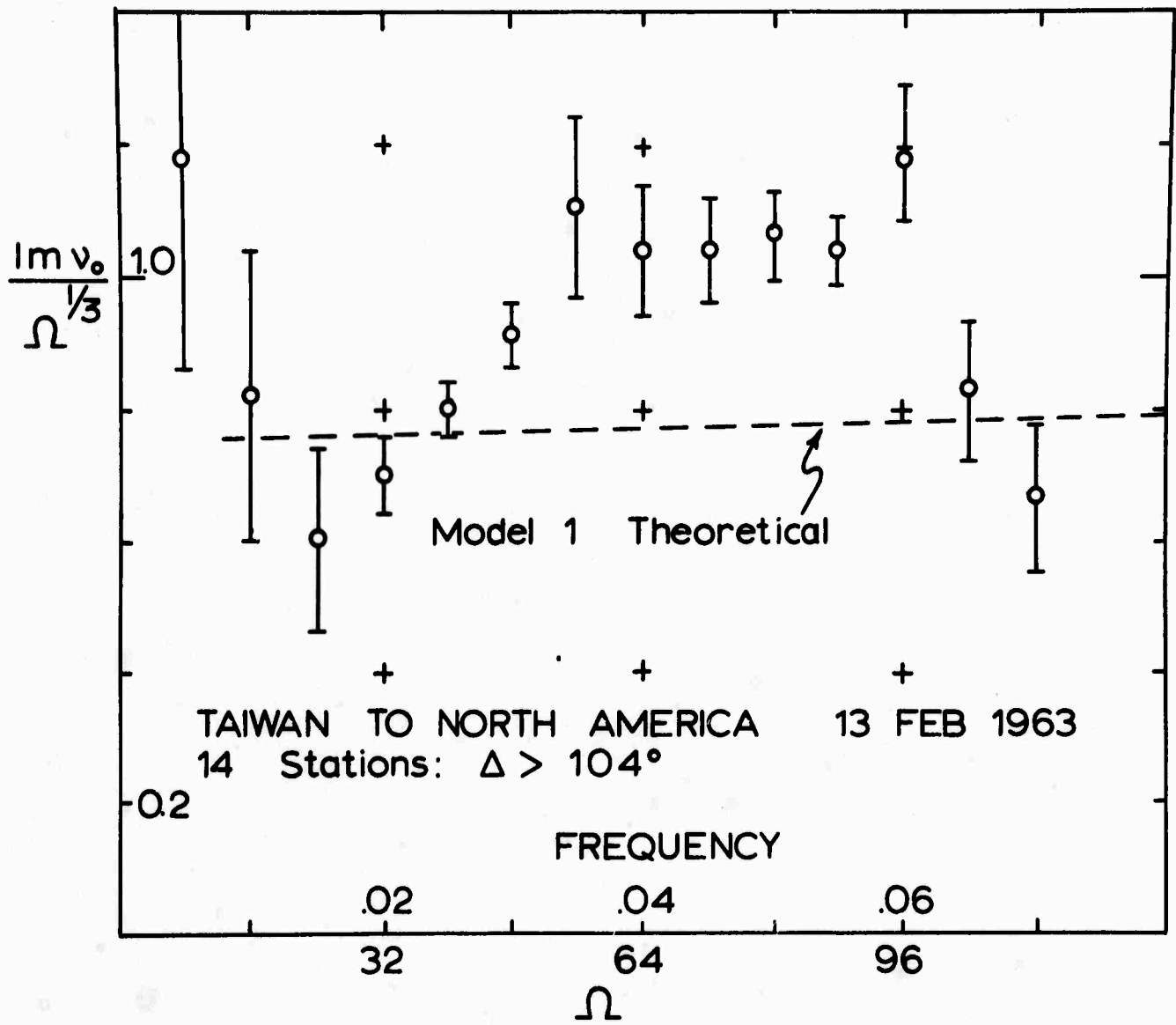


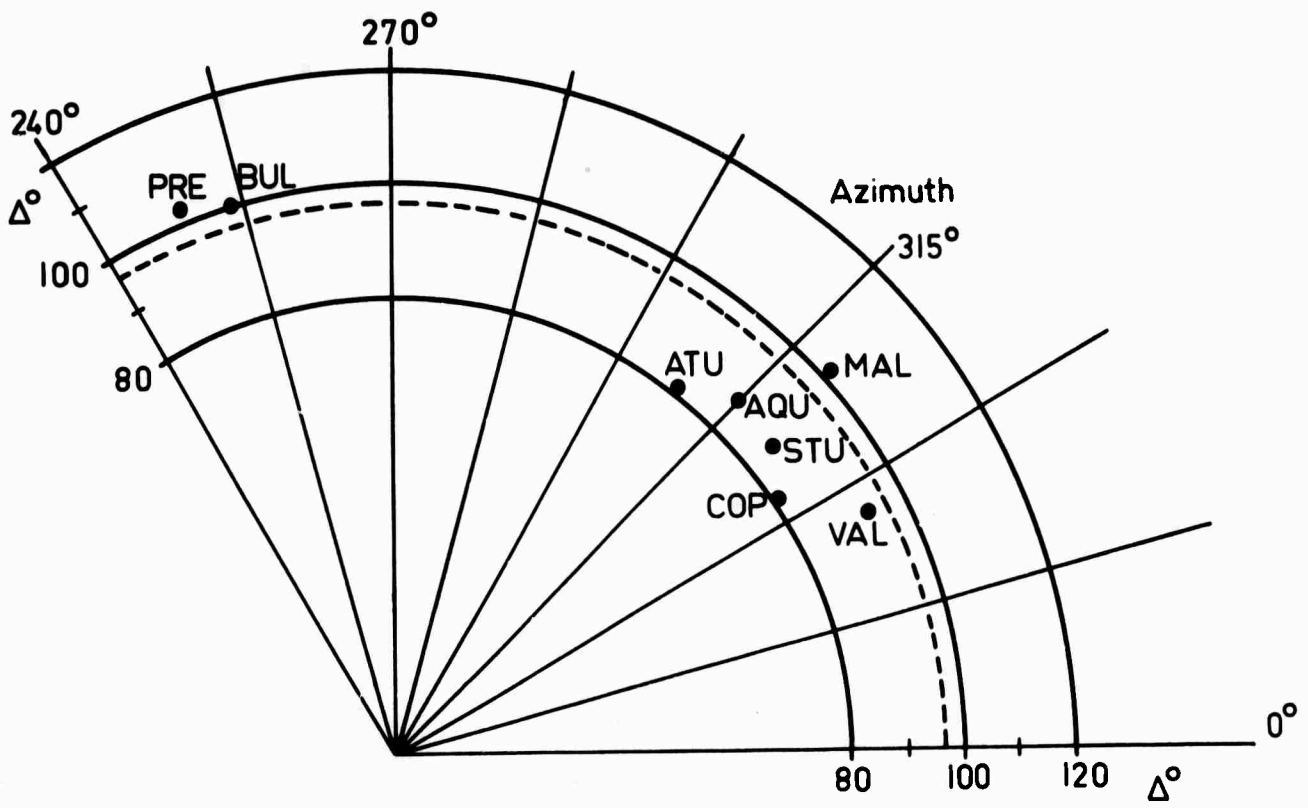
TAIWAN TO NORTH AMERICA 13 FEB 1963





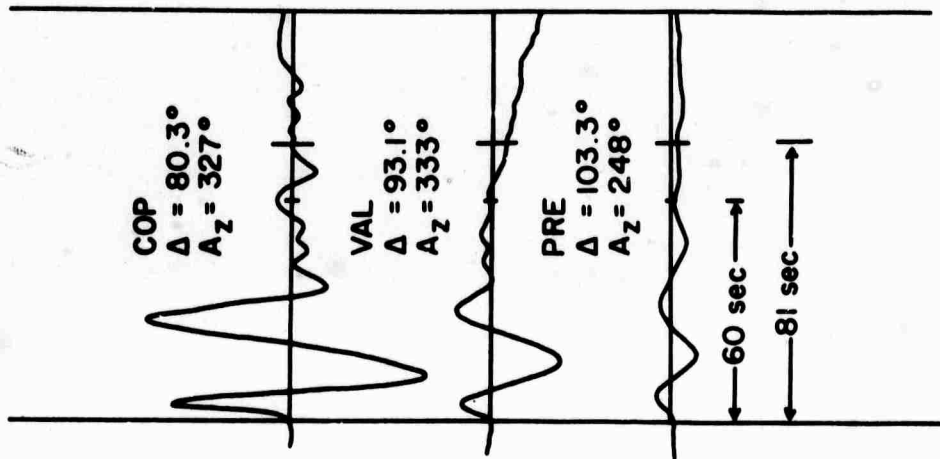
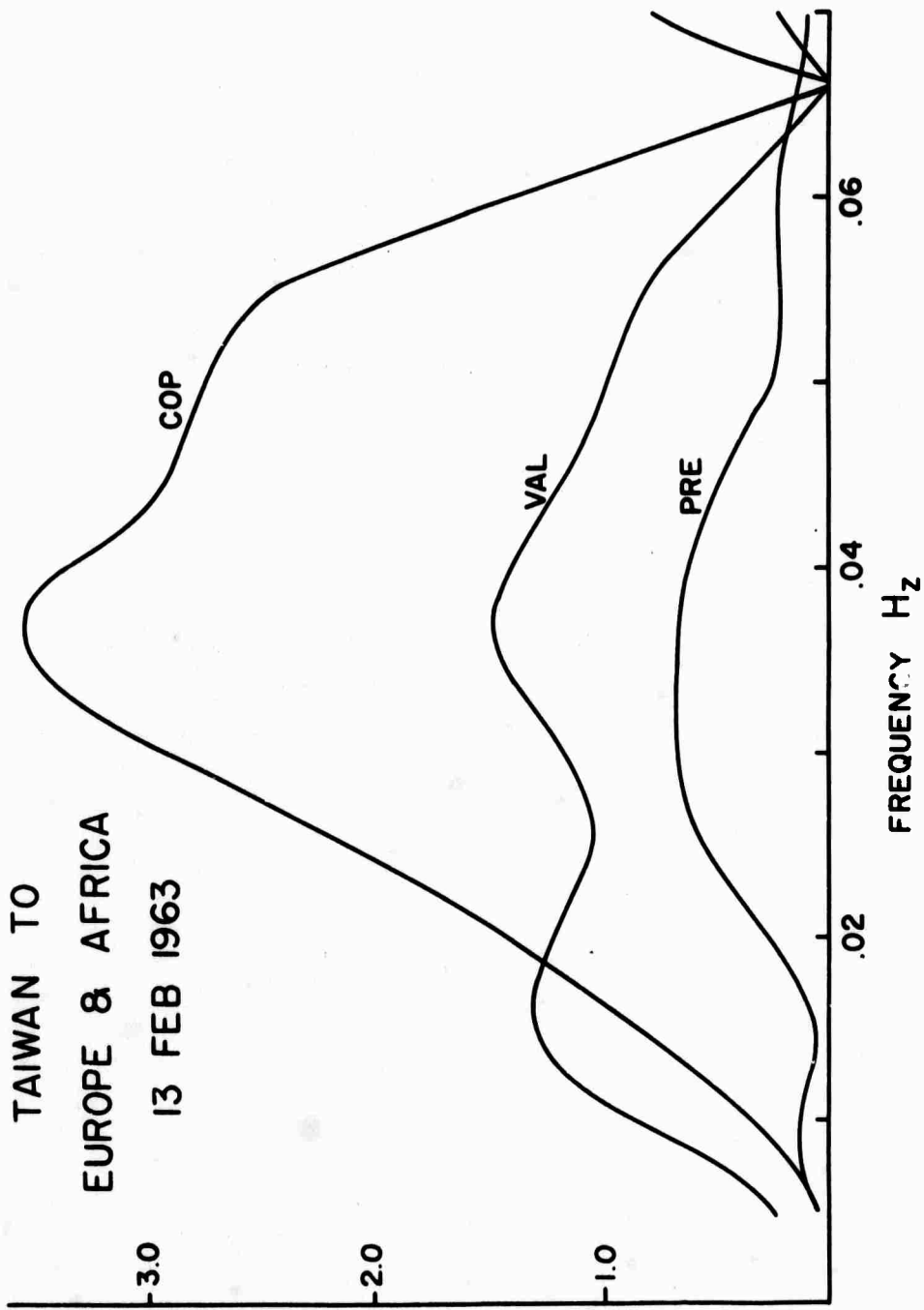
TAIWAN TO NORTH AMERICA 13 FEB 1963  
 P DIFFRACTION RESIDUALS

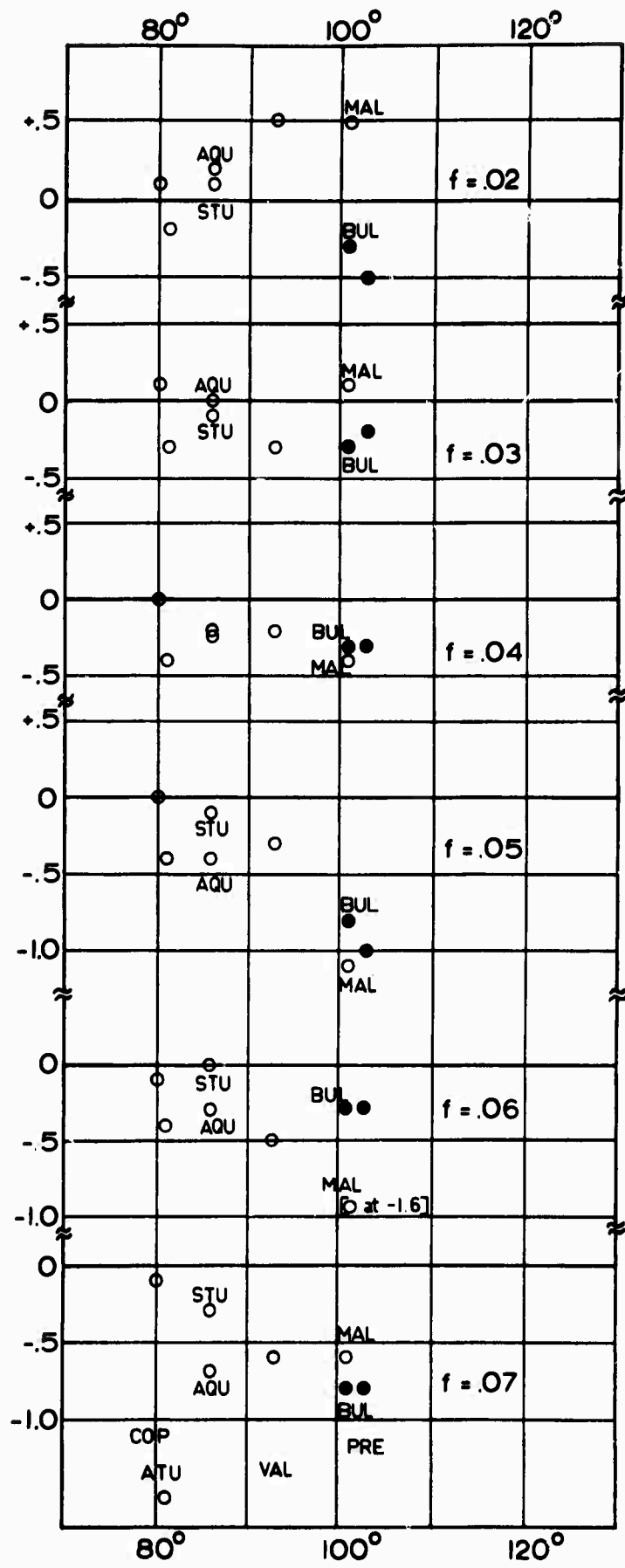




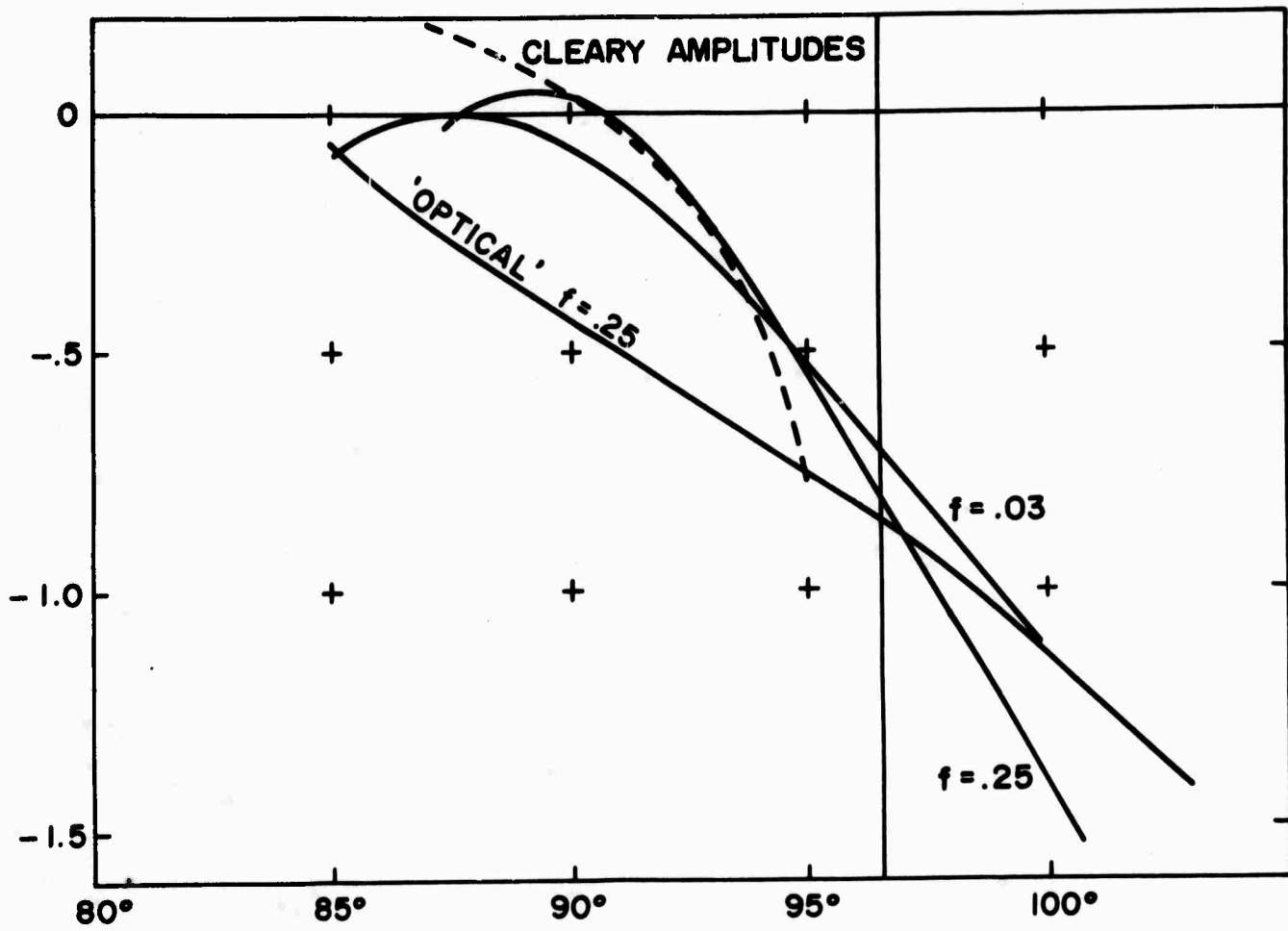
TAIWAN TO EUROPE & AFRICA 13 FEB 1963

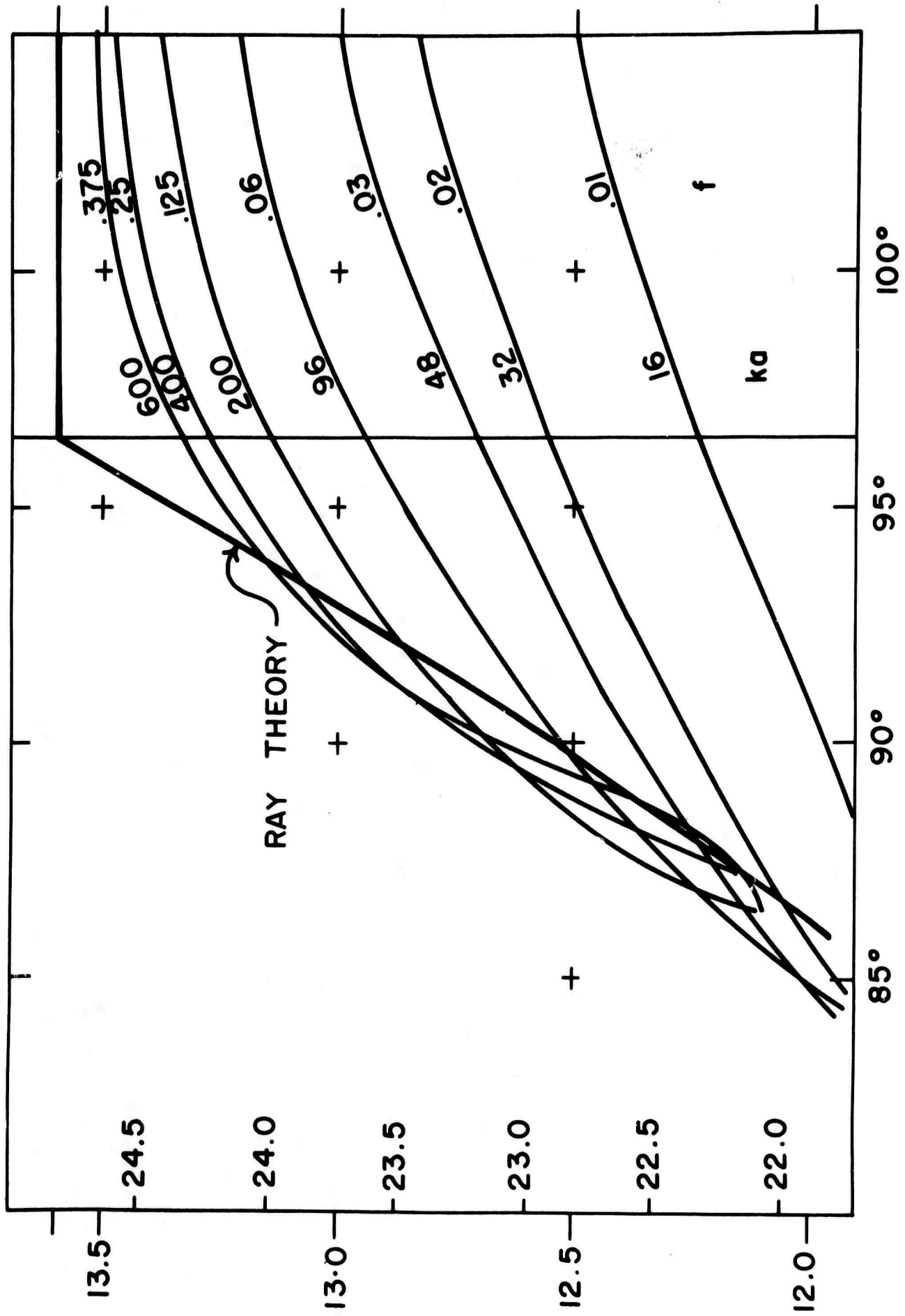
TAIWAN TO  
EUROPE & AFRICA  
13 FEB 1963

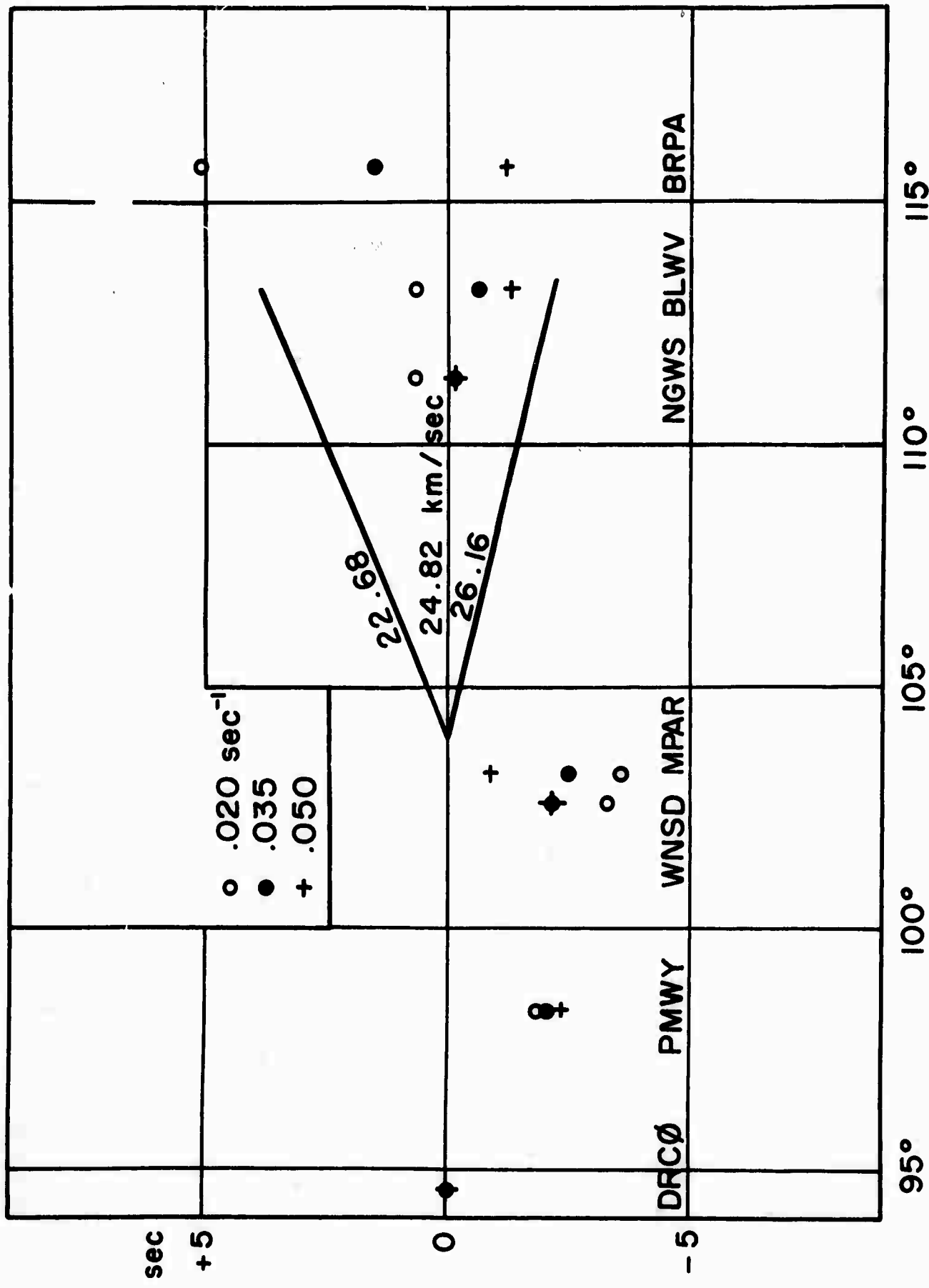




TAIWAN TO EUROPE & AFRICA 13 FEB 1963  
P DIFFRACTION RESIDUALS







. . . . .

ERRATA

1. pg. 24 Line 8 from bottom: sentence should read

Cleary also found essential agreement between his observed amplitudes and those predicted from the structure of the observed travel times (through  $d^2T/d\theta^2$ ), on a ray-theoretical interpretation.

2. Figures:  $\Delta$  should be  $\theta$   
 $A_z$  should be  $Az$   
 $H_z$  should be  $Hz$
3. Figure 16, KV should be KN

## DOCUMENT CONTROL DATA - R &amp; D

(Security classification of title, body of abstract and indexing annotation must be entered when the overall report is classified)

1. ORIGINATING ACTIVITY (Corporate author)		2a. REPORT SECURITY CLASSIFICATION	
Princeton University, Department of Geology Princeton, New Jersey 08540		UNCLASSIFIED	
		2b. GROUP	
3. REPORT TITLE			
DIFFRACTION OF P BY THE CORE: A STUDY OF LONG-PERIOD AMPLITUDES NEAR THE EDGE OF THE SHADOW			
4. DESCRIPTIVE NOTES (Type of report and inclusive dates)			
Semi annual technical summary			
5. AUTHOR(S) (First name, middle initial, last name)			
Robert A. Phinney and Lawrence M. Cathles			
6. REPORT DATE	7a. TOTAL NO. OF PAGES	7b. NO. OF REFS	
30 June 1968	64	18	
8a. CONTRACT OR GRANT NO.	8b. ORIGINATOR'S REPORT NUMBER(S)		
AF49(638)-1243	None		
8. PROJECT NO. _____			
c. 6250601R	8b. OTHER REPORT NO(S) (Any other numbers that may be assigned this report)		
d. _____			
10. DISTRIBUTION STATEMENT			
Distribution of this document is unlimited			
11. SUPPLEMENTARY NOTES		12. SPONSORING MILITARY ACTIVITY	
Submitted to J. Geophys. Res. on 23 August 1968.		Air Force Office of Scientific Research (SRPG) 1400 Wilson Blvd. Arlington, Va. 22209	
13. ABSTRACT			
<p>Theoretical expressions for the amplitude of P-waves in the neighborhood of the core shadow boundary have been formulated and evaluated by computer. Comparison with 2.5 second data of Sacks confirms his determination of the shadow position at <math>96.5^\circ</math>. A square root frequency scaling law is found for the high frequency diffraction pattern, and permits use of the Fresnel integral function at short periods. Long-period amplitude data for three paths have been spectrum analyzed and compared against the theoretical amplitude dropoff going into the shadow. The agreement is about as good as the data will permit, and no indication is found at these periods of a low-amplitude defocused region at <math>90^\circ</math> to <math>96^\circ</math>, after diffraction has been accounted for. ( )</p> <p style="text-align: right;">22209</p> <p style="text-align: center;">degrees</p>			

14.

KEY WORDS

LINK A

LINK B

LINK C

ROLE

WT

ROLE

WT

ROLE

WT

core

shadow

long-period

diffracted P

decay constant